Department of Construction Sciences
Solid Mechanics

ISRN LUTFD2/TFHF-5242/2021-SE(1-43)

Simulation of GPHE diagonal based on full material history

Master's Dissertation by

Jenny Hoang and Anna Gunnarsson

Supervisors:
Ph. D. Håkan Hallberg, Division of Solid Mechanics
M. Sc. Joakim Krantz, Alfa Laval Lund AB

Examiner:
Mathias Wallin, Division of Solid Mechanics

For information, address:
Division of Solid Mechanics, Lund University, Box 118, SE-221 00 Lund, Sweden
Webpage: www.solid.lth.se

Abstract

The objectives for this thesis is to further develop a finite element analysis methodology where the material history is evaluated in every step. The processing of the plate from coil to fully formed plate mounted in a heat exchanger should be taken into consideration. Material phenomena such as necking and springback is important to capture.

The first attempt was to do the simulation in ANSYS. This was not possible due to bugs in the software. The analysis was therefore carried out in LS-PrePost with LS-Dyna as a solver. A forming simulation, a springback analysis and a gasket simulation were performed where the springback simulation was an addition to the method, lacking from the current method performed at Alfa Laval. The forming and gasket simulation were performed with similar setup and settings as the current method with some changes to fit the purpose of this dissertation. To capture material phenomena, two material models were evaluated, Barlat 91 and YLD2000, and possible improvements to the finite element analysis was tested. The forming and the springback of the plate was analysed with the material models with 5, 7 and 11 integration points.

Even though ANSYS is a more user friendly software, the LS-Dyna method was the favorable workflow. LS-Dyna is better suited to work with metal forming and the mapping of stresses and strains between the simulations, which were important to capture the material history, were successful.

The mapping of the stresses and strains for the plates were successful and in the final gasket simulation, residual stresses and plastic strains were present, meaning that the material history is taken into consideration at the final stage. The simulations also showed different results depending on the material model and number of integration points but further analysis with physical tests are necessary to determine which model is the most similar to the actual plate.

Contents

1 Introduction

This chapter is an introduction to the dissertation and the objectives. Alfa Laval and their fluid handling technologies are presented to get a better understanding of the thesis and the gasketed plate heat exchanger that this dissertation will address. The following sections describe the limitations and further explanation of the studied geometry of the heat exchanger.

1.1 Alfa Laval

Alfa Laval is a global company founded in the province Dalarna in Sweden by Gustav De Laval and Oscar Lamm in 1883. It started as the company AB Separator and in 1963 the company became Alfa Laval. Alfa Laval has three key product areas, heat transfer, separation and fluid handling. The first heat exchanger introduced by Alfa Laval appeared in 1938 and at the same time, the research and production of heat exchangers moved to Lund, Sweden. Most of the research and development for plate heat exchangers (PHE) is still done in Lund which is also the head office of Alfa Laval.[1]

Today Alfa Laval sells its products in more than 100 countries with sales worth about 46 500 million SEK (2019). Alfa Laval holds about 3 700 patents and has more than 17 000 employees all over the world. Sustainability is central to Alfa Laval's business and they contribute to 15 of UN's 17 sustainable development goals.[1]

1.2 Background

A plate heat exchanger is using the concept of creating flow channels that separate liquids without mixing them. The PHE consists of thin corrugated plates with a pattern that will make the transfer of heat as effective as possible. The plates have openings for two fluids.

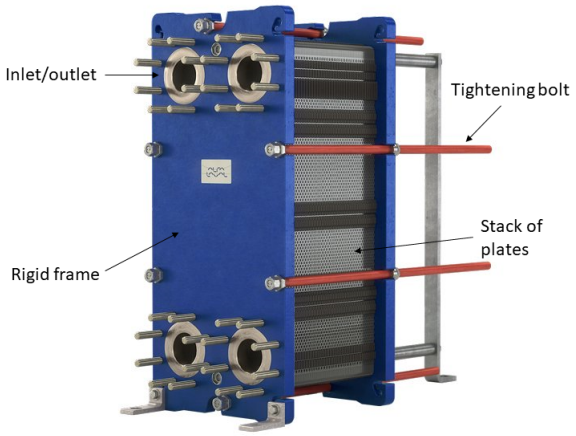

Figure 1.1: *Gasketed plate heat exchanger.*[2]

A gasketed plate heat exchanger (GPHE), figure 1.1, use gaskets to separate the plates and to create channels for the liquids. To prevent leakage, the plates are compressed with a rigid frame such that the gaskets seal the flow channels. Both the number of plates and the area of the plates determine the heat transfer. The materials for both gasket and plates as well as the gasket groove and the shape of the gasket are critical for pressure performance and which type of liquids that can be used. But it is not only the pressure performance that is important, thermal performance and formability is equally important and compromises have to be made.

1.3 Manufacturing Method - Channel Plates

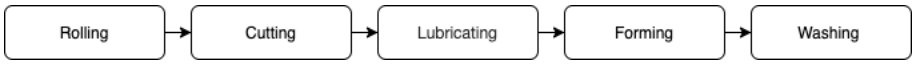

Figure 1.2: *Flow chart of the manufacturing method for the channel plates.*

The manufacturing of the plates follow the flow chart in figure 1.2. From the supplier, a rolled coil or sheet metals are prepared. The coil is cut to the dimensions of the chosen plate to prepare for forming. To make the forming process easier and to minimize the wear of the press tool the cut metal sheets are lubricated. The pattern of the press tool is meticulous designed to maximize the efficiency but still keep the thinning reasonable. After forming, the final step is to wash of the lubrication before mounting the plates in a heat exchanger.

1.4 Diagonal

The diagonal is shown in figure 1.3 and is the area of interest for this report. The diagonal is placed under the inlet and outlet of two of the four holes in a plate. The diagonal is there to stop the flow of one of the fluids. The plates are then stacked together with the two fluids on separate sides which leads to the diagonal only being present for one corner every other plate. With a high compression pressure the plates can buckle which can lead to leakage in the heat exchanger. That is why this is a particular important and interesting area.

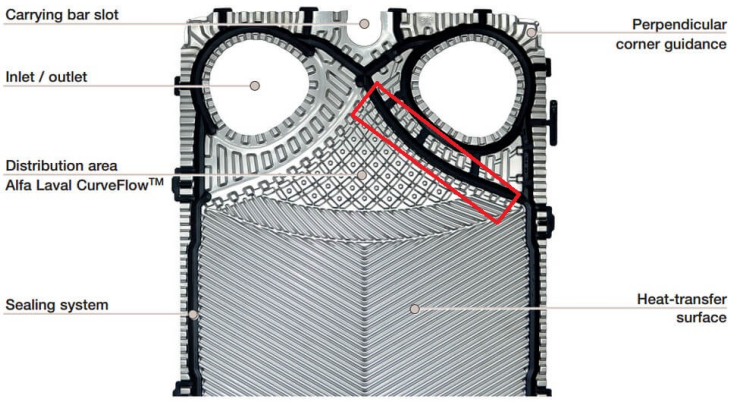

Figure 1.3: *The red box shows the diagonal.* [3]

1.5 Objectives

The aim of this thesis is to develop a finite element analysis (FEA) methodology. The processing history of the material must be considered from raw sheet or coil to fully formed plates mounted in a GPHE. The methodology developed should be a seamless solution with material history taken into consideration in every step. It is important to capture material phenomenon such as springback, necking and material thinning. The software used for the simulations are Creo Parametic for designing the geometry and ANSYS 2020 R2 and LS-PrePost V4.8.11 for the simulations.

1.6 Delimitation

One pitch of the diagonal is analyzed, as seen in figure 1.4, which is enough to determine the behaviour of the plates and gasket. For the channel plates, stainless steel grade 316 was used for the simulations and Nitrile Rubber Performance (NBR-P) for the gasket. NBR-P is an Alfa Laval unique material developed for high temperatures and it is oil and fuel resistant. Stainless steel and NBR-P are the most common materials for plates and gaskets at Alfa Laval. The diagonal which were discussed earlier in chapter 1.4 has an angle to the rolling direction of the sheet, this angle is neglected in the simulations and the diagonal is approximated to be 90 degrees to the rolling direction to facilitate the assembly of the two plates. With an angle of 90 degrees to the rolling direction, two identical plates were used instead of two mirrored plates. The beams going out from the gasket groove also have an angle to the groove, these are also neglected to make the geometry easier.

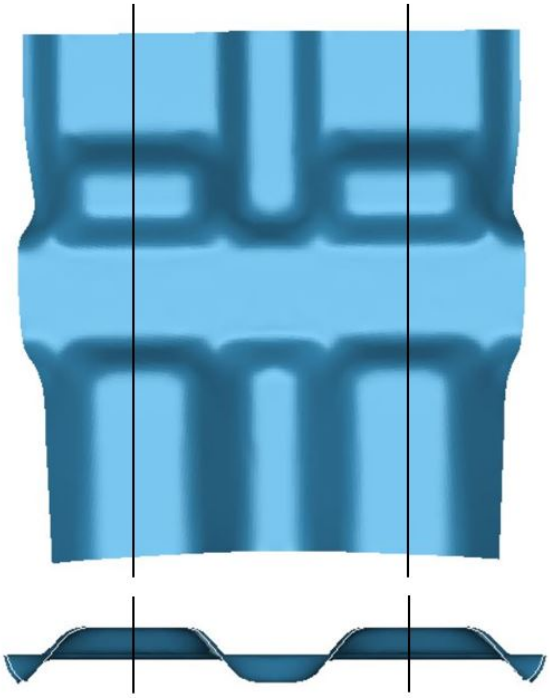

Figure 1.4: *One pitch is between the two black lines.*

2 Theory

The following chapter will explain the theory that is necessary for this dissertation which includes the finite element method but also material theory. The purpose is to give the reader a better understanding of the background and the engineering tools that has been used for the analysis. It is assumed that the reader has a basic knowledge in solid mechanics.

2.1 Finite Element Method

The finite element method is a numerical solution method commonly used for solving systems of partial differential equations. The method is quite generic but the area of interest for this project is the field of structural analysis. The method solves partial differential equations and returns an approximation to the analytical problem. By dividing the system into smaller parts, where the collection of all the parts is called the finite element mesh, the boundary value problem is rewritten as a system of algebraic equations.[4]

2.1.1 Strong Formulation

For this project, the equation of motion is used to derive the finite element formulation. The equation of motion states that all forces acting on a body is equal to the acceleration times the mass of the body. Assuming small displacements in equation 2.1

$$\int_S t_i dS + \int_V b_i dV = \int_V \rho \ddot{u}_i dV \tag{2.1}$$

where t_i is the traction vector acting on the surface $\boldsymbol{S}$, b_i is the body force per volume, ρ is the density of the body and $\ddot{u}_i$ is the second time derivative of the displacement. The strong formulation can be derived by rewriting the equation above starting with a reformulation of the surface integral. The *Gauss Divergence Theorem* formulates a relation between the flux of a vector field through a closed surface and the divergence of the field in the enclosed volume. For an arbitrary continuously differentiable vector field q_i, the *Gauss Divergence Theorem* is expressed according to the following equation 2.2:

$$\int_V q_{i,i} dV = \int_S q_i n_i dS \tag{2.2}$$

The vector can be reformulated by using the *Cauchy's formula*, equation 2.3

$$t_i = \sigma_{ij} n_j \tag{2.3}$$

where the vector n_j is the plane normal vector and σ_{ij} is the stress matrix.[4]

By combining the two equations2.2 and 2.3 and inserting in the first equation 2.1, the following expression is obtained, equation 2.4

$$\int_V (\sigma_{ij,j} + b_i - \rho \ddot{u}_i) dV = 0 \tag{2.4}$$

The expression is defined for arbitrary bodies and the balance equation can therefor be reduced to the equation below which is called the *Strong Formulation*, equation 2.5.[4]

$$\sigma_{ij,j} + b_i - \rho\ddot{u}_i \tag{2.5}$$

2.1.2 Weak Formulation

To proceed with the FE formulation, the strong form in equation 2.5 needs to be reduced to its weak form. The reduction is achieved by a weighted integration of the strong form which is a partial differential equation. The dependent variable is transferred to a weight function with the boundary conditions of the problem included in the new formulation. To establish the weak formulation, the equation of motion is multiplied by an arbitrary vector, the *weight function* v_i and integrated over the volume and can be seen in equation 2.6.

$$\int_V v_i\sigma_{ij,j}dV + \int_V v_i b_i dV = \int_V v_i\rho\ddot{u}_i dV \tag{2.6}$$

The first term is then expanded by using the rule of integration by parts derivation, equation 2.7.

$$\int_V v_i\sigma_{ij,j}dV = \int_V (v_i\sigma_{ij})_j dV - \int_V v_{i,j}\sigma_{ij}dV \tag{2.7}$$

Just like the strong formulation, the first term in the right hand side can be rewritten using the *Gauss divergence theorem*, equation 2.2, and *Cauchy's formula*, equation 2.3. Using this substitution the following equation 2.8 is derived.

$$\int_V (v_i\sigma_{ij})_{,j}dV = \int_S \sigma_{ij}v_i n_j dS = \int_S v_i t_i dS \tag{2.8}$$

By combining equation 2.7 and 2.8 and inserting in equation 2.6, the weak formulation is obtained, equation 2.9.

$$\int_S v_i t_i dS - \int_V v_{i,j}\sigma_{ij}dV + \int_V v_i b_i dV = \int_V v_i\rho\ddot{u}_i dV \tag{2.9}$$

The kinematic relation for the strain tensor known as the *Green strain* is formulated as following, equation 2.10.

$$\varepsilon_{ij} = \frac{1}{2}(u_{i,j} + u_{j,i} + (u_{k,i}u_{i,k})) \tag{2.10}$$

When assuming small strains the last quadratic term can be neglected and the equation can be written for an arbitrary vector v_i. The tensor ε^v_{ij} which has no physical significance but defines the tensor related to the vector v_i, as seen in equation 2.11.

$$\varepsilon^v_{ij} = \frac{1}{2}(v_{i,j} + v_{j,i}) \tag{2.11}$$

By inserting the equation above into equation 2.9, the weak formulation of the equation of motion is obtained, equation 2.12.[4]

$$\int_V v_i \rho \ddot{u}_i dV + \int_V \varepsilon_{ij}^v \sigma_{ij} dV = \int_S v_i t_i dS + \int_V v_i b_i dV \tag{2.12}$$

2.1.3 FE Approximation of the Weak Form

Finally, the finite element formulation can be established by first stating the weak formulation 2.12 on matrix format, which provides equation 2.13.

$$\int_V \rho \boldsymbol{v}^{\boldsymbol{T}} \ddot{\boldsymbol{u}} dV + \int_V (\boldsymbol{\varepsilon}^{\boldsymbol{v}})^T \boldsymbol{\sigma} dV = \int_S \boldsymbol{v}^{\boldsymbol{T}} \boldsymbol{t} dS + \int_V \boldsymbol{v}^{\boldsymbol{T}} \boldsymbol{b} dV \tag{2.13}$$

Where the vector components are defined according to the following definitions.

$$\boldsymbol{v} = \begin{pmatrix} v_1 \\ v_2 \\ v_3 \end{pmatrix} \ddot{\boldsymbol{u}} = \begin{pmatrix} \ddot{u}_1 \\ \ddot{u}_2 \\ \ddot{u}_3 \end{pmatrix} \boldsymbol{\varepsilon}^{\boldsymbol{v}} = \begin{pmatrix} \varepsilon_1^v \\ \varepsilon_2^v \\ \varepsilon_3^v 3 \\ 2\varepsilon_{12}^v \\ 2\varepsilon_{13}^v \\ 2\varepsilon_{23}^v \end{pmatrix}$$

$$\boldsymbol{\sigma} = \begin{pmatrix} \sigma_1 \\ \sigma_2 \\ \sigma_3 \\ \sigma_{12} \\ \sigma_{13} \\ \sigma_{23} \end{pmatrix} \boldsymbol{b} = \begin{pmatrix} b_1 \\ b_2 \\ b_3 \end{pmatrix} \boldsymbol{t} = \begin{pmatrix} t_1 \\ t_2 \\ t_3 \end{pmatrix}$$

The discrete Galerkin formulation can be achieved by first introducing an approximated relation to the displacement $\boldsymbol{u}$. The displacement $\boldsymbol{u}$ is expressed using the approximated relation called *global shape function* $\boldsymbol{N}$, which relates the element displacement at any point of the element to the *nodal displacement*. With an interpolation function, the displacement at any point of the element can then be calculated which also result in the possibility of calculating the displacement throughout the body at any time and location. The vector for the displacement is a function of the position $\boldsymbol{a}$ and the shape functions. See equation 2.14 below.

$$\boldsymbol{u}(x_i, t) = \boldsymbol{N}(x_i)\boldsymbol{a}(t) \tag{2.14}$$

The interpolation between the nodal displacement and the displacement vector depends on the approximation method. The Green strain expression 2.10 can be specified as following in equation 2.15.

$$\varepsilon(x_i, t) = \boldsymbol{B}(x_i)\boldsymbol{a}(t) \tag{2.15}$$

The *global kinematic matrix* $\boldsymbol{B}(x_i)$ contains the spatial derivatives of the shape functions. The remaining vector to declare is the weight function which will also be defined according to the *Galerkin method*. The approximation of the weight vector is expressed in equation 2.16

$$\boldsymbol{v}(x_i, t) = \boldsymbol{N}(x_i)\boldsymbol{c}(t) \tag{2.16}$$

where the vector $\boldsymbol{c}$ is an arbitrary vector. By using the relation between $\boldsymbol{\varepsilon}$ and $\boldsymbol{u}$, the weighted strain $\boldsymbol{\varepsilon^v}$ can be defined as equation 2.17

$$\boldsymbol{\varepsilon^v} = \boldsymbol{Bc} \tag{2.17}$$

The previously defined variables can be inserted into the weak formulation to achieve following equation, equation 2.18

$$\boldsymbol{c^T}[(\int_V \rho \boldsymbol{N^T N} dV)\ddot{\boldsymbol{a}} + \int_V \boldsymbol{B^T}\boldsymbol{\sigma} dV - \int_S \boldsymbol{N^T t} dS - \int_V \boldsymbol{N^T b} dV] = 0 \tag{2.18}$$

Finally, the stress is also rewritten to complete the finite element formulation. The stress can be defined by using the previous constitutive relation, equation 2.18, together with equation 2.10 which combined gives us equation 2.19.[4]

$$\boldsymbol{\sigma} = \boldsymbol{D\varepsilon} = \boldsymbol{DBa} \tag{2.19}$$

The stress is inserted in the expression above and since $\boldsymbol{c}$ is an arbitrary vector, the expression inside the branches in equation 2.18 must be equal to zero which lead to the following expression.

$$(\int_V \rho \boldsymbol{N^T N} dV)\ddot{\boldsymbol{a}} + (\int_V \boldsymbol{B^T D B} dV)\boldsymbol{a} - \int_S \boldsymbol{N^T t} dS - \int_V \boldsymbol{N^T b} dV = 0 \tag{2.20}$$

The final finite element formulation is obtained by rewriting the expression into a more compact format, appearing as

$$\boldsymbol{M}\ddot{\boldsymbol{a}} + \boldsymbol{Ka} = \boldsymbol{f} \tag{2.21}$$

where

$$\textit{The mass matrix}: \boldsymbol{M} = \int_V \rho \boldsymbol{N^T N} dV \tag{2.22}$$

$$\textit{The stiffness matrix}: \boldsymbol{K} = \int_V \boldsymbol{B^T D B} dV \tag{2.23}$$

$$\textit{The external force vector}: \boldsymbol{f} = \int_S \boldsymbol{N^T t} dS + \int_V \boldsymbol{N^T b} dV \tag{2.24}$$

The first term in the finite element formulation is only used in dynamic simulations where calculations are time-dependent. The boundary conditions to the formulation contain prescribed conditions to the body, which can be displacement or a traction vector acting along a certain boundary surface. For time-dependent problems, also initial values must be prescribed.[4]

2.2 Large Deformation

Small deformations are defined by an initial configuration. To end up at the current configuration, a displacement vector u is added, as seen in figure 2.1.

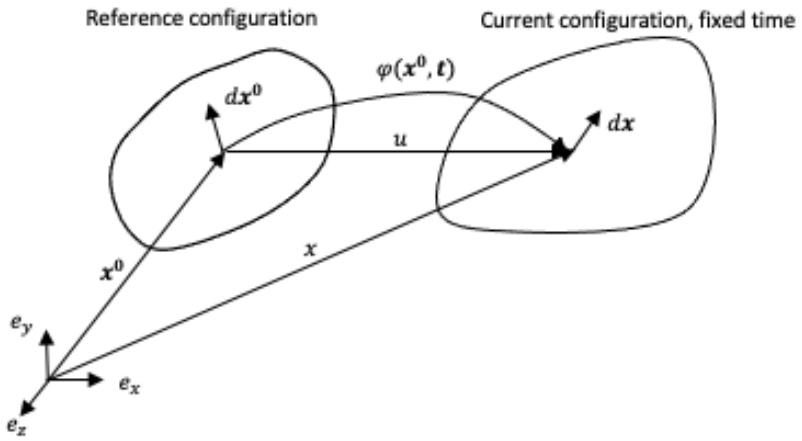

Figure 2.1: *Displacement* $\boldsymbol{u}$ *from reference configuration* $\boldsymbol{x_0}$ *to current configuration* $\boldsymbol{x}$*. Reproduced from Ristinmaa, M.. 'Introduction to Non-linear Finite Element Method'* [6]*.*

Large deformations on the other hand uses a deformation gradient tensor $\mathbf{F}$ to map vectors from one configuration to another. The deformation gradient follows equation 2.25 since $x = x(x_0, t)$

$$d\boldsymbol{x} = \boldsymbol{F} d\boldsymbol{x_0} \tag{2.25}$$

where x is the current configuration and x_0 is the reference configuration. To determine the strain tensor, equation 2.26, equation 2.10 is used which is known as the Green's strain tensor

$$\boldsymbol{E} = \frac{1}{2}(\boldsymbol{C} - \boldsymbol{I}) \tag{2.26}$$

where $\boldsymbol{I}$ is the identity tensor and $\boldsymbol{C}$ is the right Cauchy-Green tensor, which is found from equation 2.27.

$$\boldsymbol{C} = \boldsymbol{F^T F} \tag{2.27}$$

The strain matrix $\boldsymbol{E}$ is symmetric whereby it can be written as a vector on the following

format.

$$E = \begin{pmatrix} E_{xx} \\ E_{yy} \\ E_{zz} \\ 2E_{xy} \\ 2E_{yz} \\ 2E_{xz} \end{pmatrix} \tag{2.28}$$

To determine the stress for large deformation the *Piola-Krichoff tensors* is used. Again Cauchy's formula is used to define a tensor, but this time in the reference configuration and are derived in equation 2.29.

$$\boldsymbol{t_0} = \boldsymbol{P}\boldsymbol{n_0} \tag{2.29}$$

This tensor is a second order tensor named *first Piola-Kirchhoff stress tensor*. This equation together with Cauchy's stress tensor holds a relation as following in equation 2.30

$$\boldsymbol{P} = J\boldsymbol{\sigma}\boldsymbol{F}^{-\boldsymbol{T}} \tag{2.30}$$

where J is the *Jacobian* defined in 2.31 and represents the volume change during deformation

$$J = det\boldsymbol{F} \tag{2.31}$$

The first Piola-Krichhoff stress tensor is not symmetric and therefore the *second Piola-Kirchhoff stress tensor* is introduced, which is defined in equation 2.32

$$\boldsymbol{S} = J\boldsymbol{F}^{-\boldsymbol{1}}\boldsymbol{\sigma}\boldsymbol{F}^{-\boldsymbol{T}} \tag{2.32}$$

The *second Piola-Krichhoff stress tensor* is symmetric and can be written as a vector and is shown on matrix format in 2.33.[5]

$$S = \begin{pmatrix} S_{xx} \\ S_{yy} \\ S_{zz} \\ S_{xy} \\ S_{yz} \\ S_{xz} \end{pmatrix} \tag{2.33}$$

2.3 Plasticity Theory

For an elastic material, a loaded body returns to its original shape when unloaded but for many cases the body is left with residual strains, also called plastic strains. The plasticity theory covers linear and nonlinear time-independent behavior where residual strains exist when unloading a body. Plastic strains are developed when the loading exceeds a materials yield stress σ_y and the behavior when the stress $\sigma > \sigma_y$ is described by a yield function f, which is a material dependent function. The yield function can be used to define yield surface. The yield surface varies with the plastic loading and the change of the yield surface

is related to the hardening behavior of the material. The hardening of a material is a typical characteristic for steel alloys as the yield stress is increased with increasing plastic strain. The following expression describes the *current yield surface*

$$f(\sigma_{ij}, K_1, K_2, ...) = 0 \tag{2.34}$$

where $K_1, K_2, ...$ are the *hardening parameters* which characterize the change in size, shape and position of the current yield surface for a certain material. For the initial state the hardening parameter $K_a = 0$.[5,6]

2.3.1 Isotropic Hardening

If the loading past the yield strength expands the yield surface but the surface remains at the same position and shape, the hardening is denoted *isotropic hardening*. See figure 2.2 below.

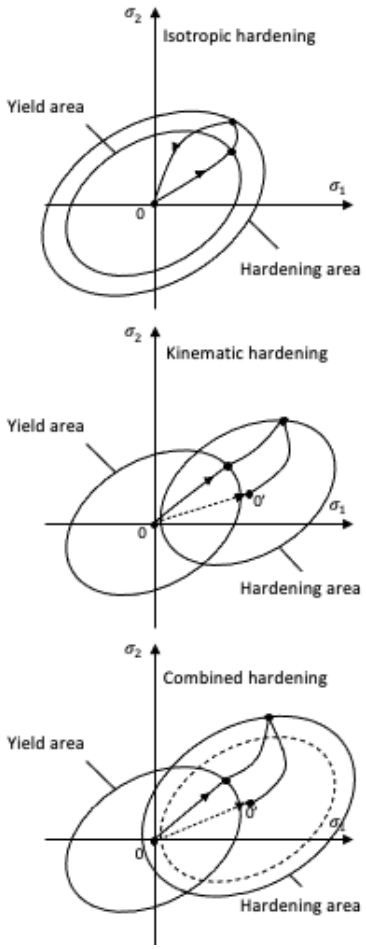

Figure 2.2: *Change in yield surface for isotropic, kinematic and lastly the combined hardening. Reproduced from presentation material provided by Dynamore Nordic.*

As seen in the figure 2.2, the isotropic hardening model implies that the yield strength is

symmetric about the hydrostatic axis if the the yield strength in tension and compression are initially the same. The shape is maintained as the yield surface increases with the plastic strain. The general yield function is described by the following function

$$f(\sigma_{ij}, K_i) = f_0(\sigma_{ij}) - K = 0 \tag{2.35}$$

where the yield function is specified by the initial yield function and the *hardening parameter* K. [6]

2.3.2 Kinematic Hardening

If loading past the yield strength translates the yield surface from its original position in the stress space, the hardening is denoted *kinematic hardening*. The hardening rule enables modeling of responses where the hardening in tension will lead to softening in a subsequent compression, an example on this type of response is the Bauschinger effect. Kinematic hardening is typically relevant for scenarios involving cyclic loading. The general yield function for the kinematic hardening takes the form

$$f(\sigma_{ij}, K_i) = f_0(\sigma_{ij} - \alpha_{ij}) = 0 \tag{2.36}$$

The function is described by the *back-stress* α_{ij}. The yield surface shifts relative to the stress axes by α_{ij} .

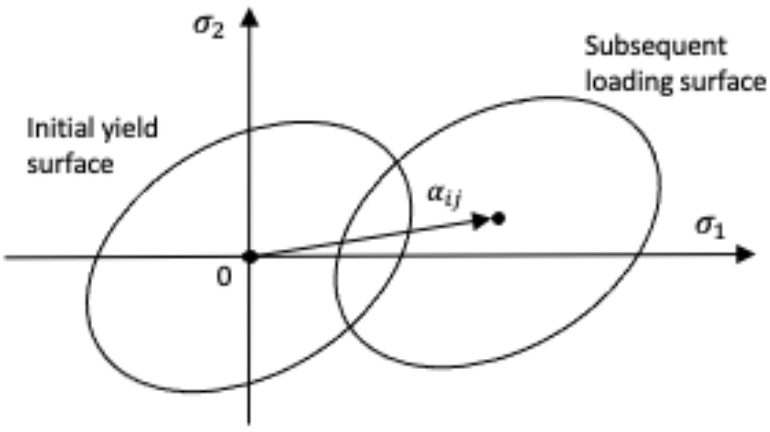

Figure 2.3: *The yield surface shift by the back-stress. Reproduced from Ristinmaa, M.. 'Introduction to Non-linear Finite Element Method'* [6].

The *combined or mixed hardening* rule combines the characteristics of both the isotropic and the kinematic hardening models. The function is described by the following, equation 2.37.

$$f(\sigma_{ij}, K_i) = f_0(\sigma_{ij} - \alpha_{ij}) - K = 0 \tag{2.37}$$

The hardening parameters are now the scalar K and the tensor α_{ij}.[6]

2.4 Material Phenomenon

2.4.1 Springback

When working with the elastic-plastic characteristics of metals, certain phenomena needs to be accounted for during the design and manufacturing. For sheet metal forming, one such phenomenon is *springback*. Springback is a geometrical change that occur when the component is removed from the die. The elastic deformation of the sheet is released as it is released from the forces from the die and only the plastic deformation will remain. This causes difficulties with meeting the dimensional specifications and requires accurate material models and simulations to predict the springback of a material. [7]

2.4.2 Necking

Another phenomenon to take into account is the *necking* of a material. Necking occurs when the cross-section area is greatly reduced. The formation of strain hardening occurs when the material undergoes tensile deformation past the ultimate strength, see figure 2.4. This results in an exclusive area of yielding since the reduced cross-section leads to the largest local stress. The phenomena is geometrical unstable and will continue to deform at the concentrated stress area until the material ruptures. In sheet metal forming, the formation of necking in different areas of the material leads to *material thinning*. [8]

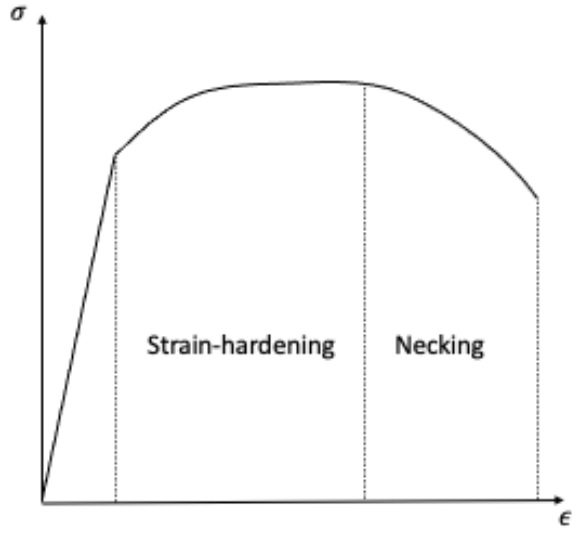

Figure 2.4: *Stress-strain curve where the later part of the curve shows the area of necking.*

2.5 Contacts

This project focuses on the methodology on how to capture physical phenomenon and the result is affected by many factors. However, since the task is to mainly develop a method and the result is not primarily affected by the contact method, the report will only introduce a short definition of contacts in FEM and the method that is used.

The interaction between different parts can be calculated using contact algorithms. There are different methods to find the contact between elements but also to assign the contact forces that occur in reality such as frictional forces. The most commonly used contacts are based on the penalty method. The parts in contact are defined as either a master or a slave, which can either have a non symmetric or a symmetric behavior. For a non symmetric contact, the slave side is defined by nodes and the master side by segments and only the slave nodes are checked against penetration. Figure 2.5 demonstrates the different behavior depending on which part is assigned as slave or master. For the symmetric contact, the behavior is independent of the selection of master or slave since both is checked against penetration. For the gasket simulation performed in LS-Dyna, the automatic surface to surface mortar method is used and is symmetric, include self contact and is sensitive to initial penetrations and suitable for implicit simulations.[9]

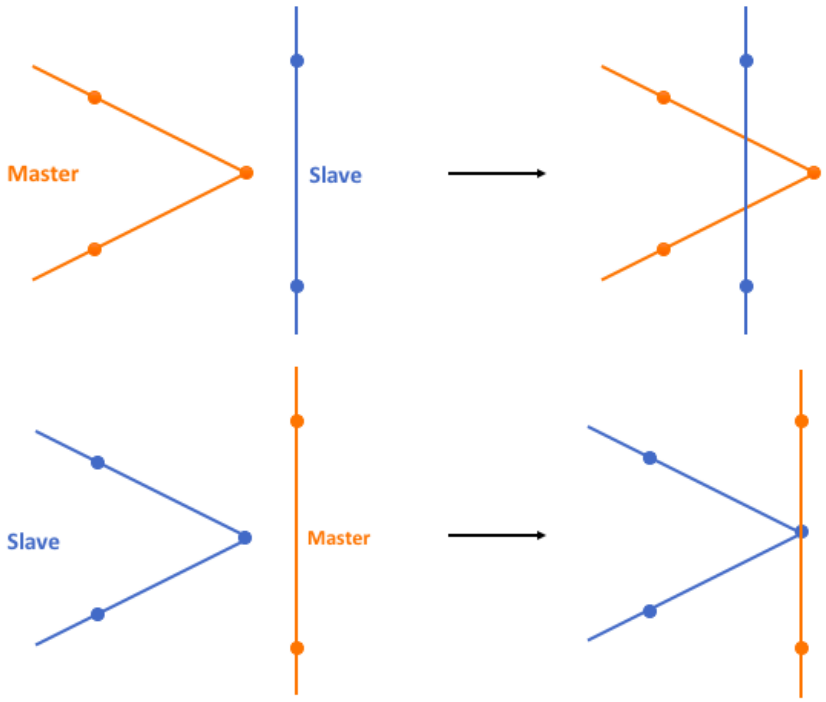

Figure 2.5: *Non-symmetric contacts where the upper part of the figure shown a contact where the segments of the master part checks for nodes on the slave part and penetration occurs. The second part of the figure shows the nodes of the slave part checking for segments on the master part and no penetration occurs.*

2.6 Material Models

To predict the geometry and mechanical properties of components, it is necessary to perform structural analyses by using the Finite element method (FEM). A Finite element analysis is both cost and time efficient compared to other methods for instance physical tests based on trial-and-error but the accuracy and precision of the method is highly dependant on the constitutive model describing the behavior of the material. To capture local phenomena such as necking in the sheet forming process, the material history is taken into consideration which for rolled sheet metals includes anisotropic characteristics. Anisotropic material behavior is when a material have different properties in different directions.[6]

2.6.1 Barlat 91

The material model Barlat 91, developed by Frederic Barlat[10] aims to model sheets under plane stress conditions with anisotropy. Lankford parameters[10], seen in equation 2.38 are used to define the yield surface. A Lankford parameter is a scalar that measure the plastic anisotropy of a sheet metal. It indicates the formability in the different directions.

$$R_\alpha = \frac{\varepsilon_w^p}{\varepsilon_t^p} \tag{2.38}$$

The yield criterion, equation 2.39 can be written as

$$\overline{\sigma}(\sigma) = 2^{\frac{-1}{M}}(a(K_1 - K_2)^M + a(K_1 + K_2)^M + c(2K_2)^M)^{\frac{1}{M}} \tag{2.39}$$

where the K_1 and K_2 parameters are defined in the following equations.

$$K_1 = \frac{\sigma_{11} + h\sigma_{22}}{2} \tag{2.40}$$

$$K_2 = \sqrt{(\frac{\sigma_{11} - h\sigma_{22}}{2})^2 + p^2\sigma_{12}} \tag{2.41}$$

The parameters a, c, p and h can be determined from the Lankford parameters and trough yield stress.[10] The parameter M determines the shape of the yield surface and a higher value of M makes it look more like von Mises and a lower value makes it look like Tresca.

2.6.2 Barlat YLD2000

Barlat YLD 2000 is a model derived by Frederic Barlat and the yield criterion is determined by the following, equation 2.42.

$$\Phi' + \Phi'' = 2(\overline{\sigma})^a \tag{2.42}$$

where

$$\Phi' = (X_1' - X_2') \tag{2.43}$$

$$\Phi'' = (2X_2'' - X_1'')^a + 2(2X_1'' - X_2'')^a \tag{2.44}$$

This can be formulated by either anisotropy parameters or by stress points and Lankford parameters. This material model includes kinematic hardening. This material model is better at estimating springback. The yield functions for Von Mises, Hill'48 and Barlat YLD2000 are shown in figure 2.6.[11]

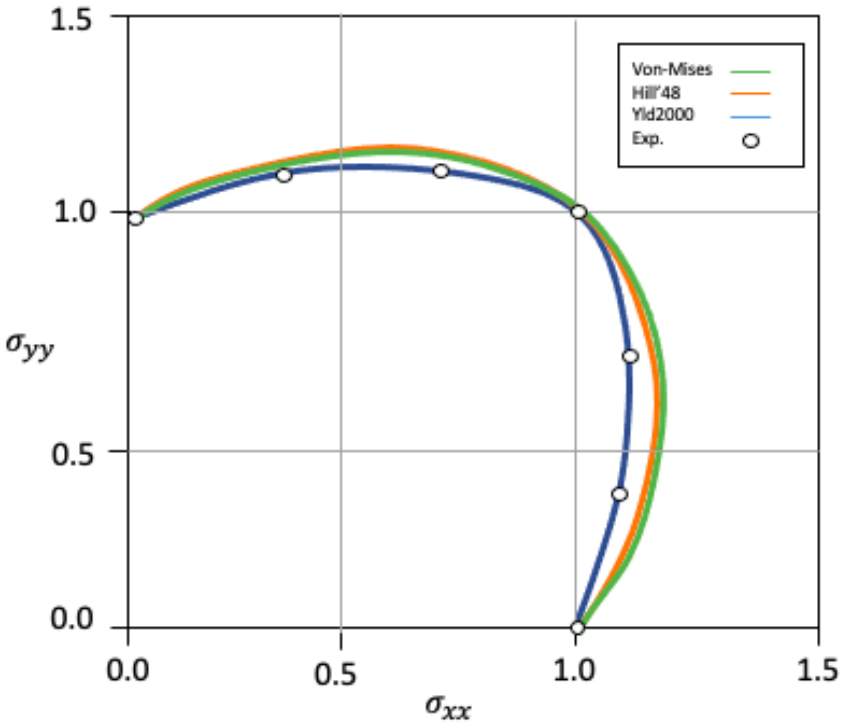

Figure 2.6: *Comparison of experimental data with theoretical material models. Reproduced from presentation material provided by Dynamore Nordic.*

2.6.3 Hyperelastic Material

Hyper-elasticity is a constitutive relation that is a special case of a Cauchy elastic material and is derived by considering the strain energy. The relation provides a stress-strain relation which can be formulated as suitable for nonlinear, isotropic and incompressible materials such as rubber material. The Neo-Hookean and Mooney-Rivlin solids are two material models developed for hyperelastic materials.[6]

2.7 Element Theory

In the simulations, two elements were used by the ANSYS software. One for the sheet metal and one type for the gasket. The sheet metal was declared as a sheet geometry and therefore uses shell elements and the gasket is a solid and therefore uses solid elements.

2.7.1 Isoparametic mapping

Isoparametric mapping allows for an undeformed isoparametric element in a local $\xi\eta$-coordinate system to be defined as the deformed element in the global xy-coordinate system. In other words, the elements in the *parent domain* can be mapped to a *gloabal domain*, figure 2.7. Since the isoparametric elements and the corresponding shape functions are now defined in the $\xi\eta$-coordinate system, one encounters problems when defining the stiffness matrix $\boldsymbol{K}$. As seen in the expression 2.23, the stiffness matrix is defined by the $\boldsymbol{B}$-matrix which is obtained by differentiating the shape function $\boldsymbol{N}$ with respect to the coordinates in the global domain. The differentiated shape functions leads to integrals that are difficult to solve analytically but can be approximated and solved by using *numerical integration techniques*.[4]

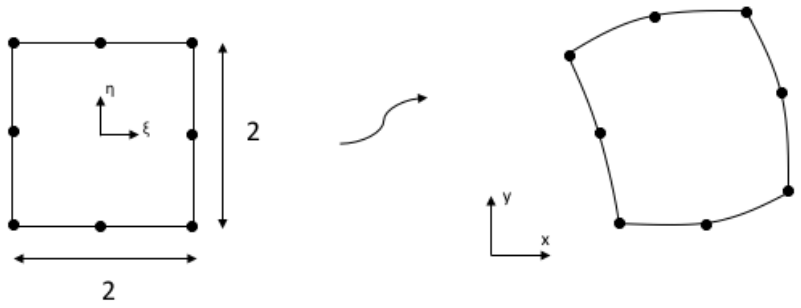

Figure 2.7: *Isoparametric mapping of an element from the parent domain to the global domain. Reproduced from Ottosen, N., Peterson, H., 'Introduction to the finite element method'*[4].

2.7.2 Gauss integration points

When dealing with isoparametric element, a numerical integration technique needs to be used to solve the integrals. A commonly used numerical integration technique to solve integrals is the *Gauss integration scheme*. This section will briefly go through the method. Consider the general integral in equation 2.45,

$$H = \int_{-1}^{1} h(x) = dx \tag{2.45}$$

where $h(x)$ is the function and H is the integration quantity that is difficult to solve analytically. The function $h(x)$ is multiplied by a weight function w_g and the function in the integration scheme can be formulated as equation 2.46

$$H \approx \sum_{g=1}^{n_q} w_g h(x_g) \tag{2.46}$$

where the function $h(x)$ is evaluated at n_q distinct integration points, x_g and $g = 1, ..., n_q$. Dependant on the choice of position of the integration points and weight function, the variables can be chosen to achieve an exact integration of the polynomial. The Gauss

integration provides an exact integration of a polynomial of a higher order than obtained by Newton-Cotes integration. The position of the points are called *Gauss points* and an exact solution is referred to a *full integration.* It is shown that

For n integration points, Gauss integration provides an exact integration of a polynomial of the order 2n-1.[4]

In practice, Gauss integration is used almost exclusively within isoparametric FE formulations. Dependent on the physical analysis, it is important to choose the number of element carefully for the simulation. Using fewer number of integration points can be sufficient for a linear elastic material and more integration points would increase the runtime without necessarily increase the accuracy. However, when working with plastic bending behavior and different physical phenomenon, using more integration points is necessary. It is recommended to use five integration points to capture the bending of a metal during sheet metal forming and seven up to eleven integration points are necessary when analysing springback. [12]

2.7.3 Shell Formulation

This type of elements are used for thin sheets and are well-suited for nonlinear analyses with large deformations. The shell elements used in the simulations are four-node elements with six degrees of freedom with translation in x-, y- and z-direction and rotation about x-, y- and z-axes. The shell element used in the simulation is shown in figure 2.8.[9]

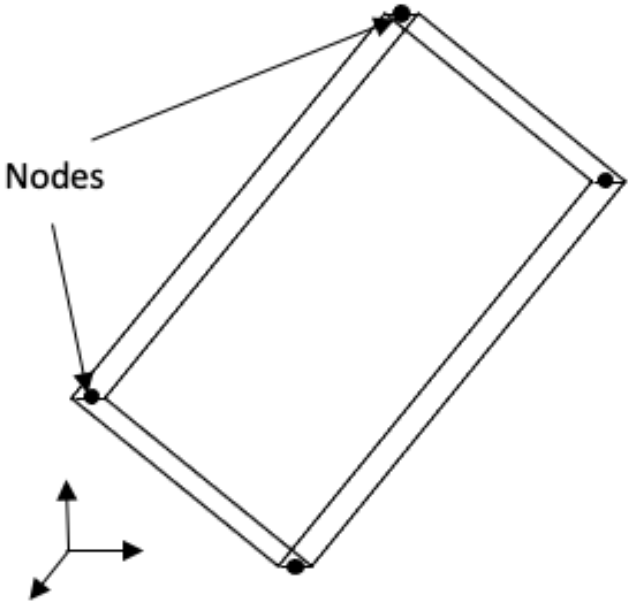

Figure 2.8: *Shell element with four corner nodes. Reproduced from 'LS-Dyna user's manual'* [9] *figure 18-25.*

2.7.4 Solid Formulation

Solid elements are used for 3D structures. For irregular regions it allows for complex shapes of the elements. The solid element in the simulations are eight-node elements that suits well for large deformations and large strains and is shown in figure 2.9. It also has the capability for simulating materials with fully incompressible hyperelastic behaviour.[9]

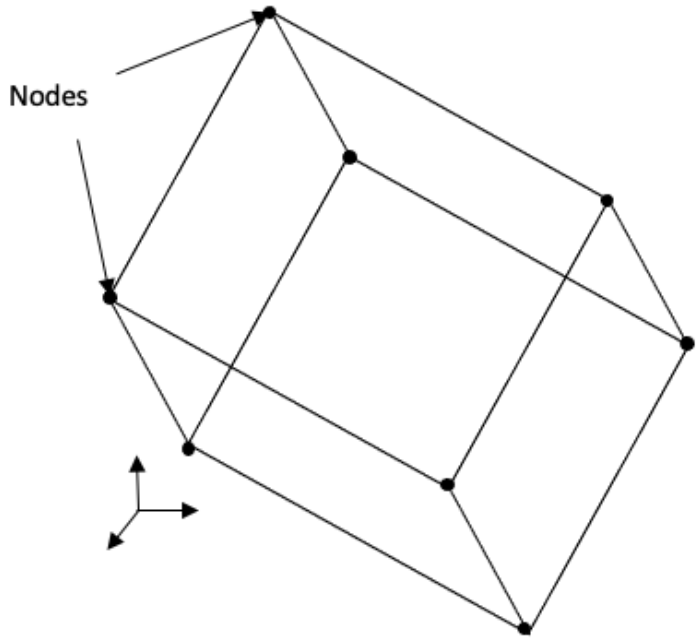

Figure 2.9: *Solid element with eight nodes. Reproduced from 'LS-Dyna user's manual' [9] figure 18-30.*

2.7.5 Hourglass

Hourglassing is an instability where elements have zero strain and it is a phenomena where the elements are buckling. Most element formulations are under-integrated, which is shown to the left in figure 2.10, which means that the stresses and strains are only calculated in one point in the element. A fully integrated element is shown in figure 2.10 to the right with four points where the stresses and strains are calculated. The advantage with under-integrated elements are the efficiency in number of computations.

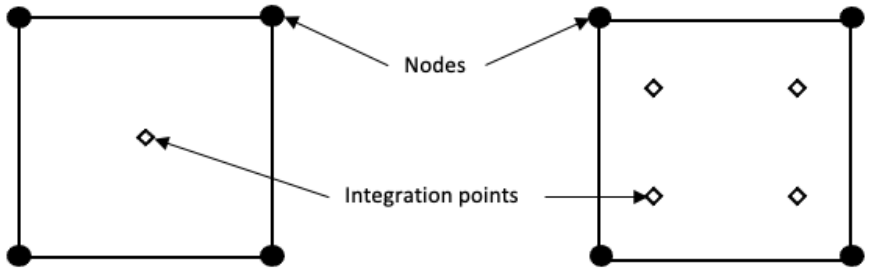

Figure 2.10: *Under-integrated shell element with one integration point (left) and fully integrated shell element with four integration points (right). Reproduced from presentation material provided by Dynamore Nordic.*

But as seen in figure 2.11 there are stress loads which can be missed. The deformation doesn't yield any strains for the integration point in the middle and therefore no stress occurs.

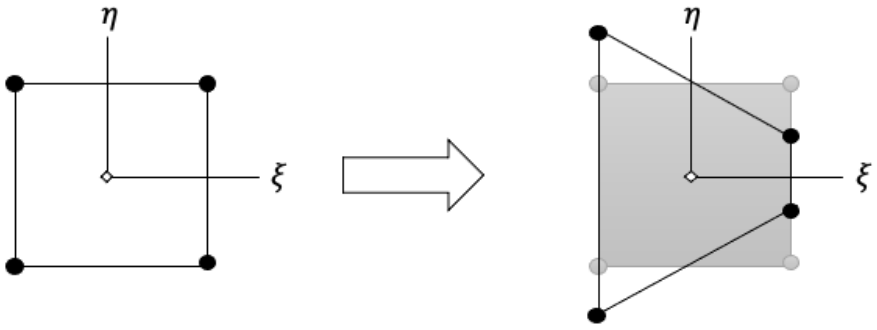

Figure 2.11: *Under-integrated shell element (left) with a deformation (right). Reproduced from presentation material provided by Dynamore Nordic.*

To prevent this from happening, one solution is to refine the mesh and a second possibility is as mentioned earlier to change to a fully integrated element, which however will make the simulation more expensive.[13]

2.8 Implicit and Explicit Methods

For implicit and explicit methods, the problems can be expressed through partial differential equations. A nonlinear problem can be expressed as following

$$\boldsymbol{M}\boldsymbol{x}'' + \boldsymbol{C}\boldsymbol{x}' + \boldsymbol{K}\boldsymbol{x} = \boldsymbol{f} \tag{2.47}$$

where $\boldsymbol{M}$ is the mass matrix, $\boldsymbol{C}$ is the Rayleigh matrix and $\boldsymbol{K}$ is the stiffness matrix.[14]

2.8.1 Implicit Method

There are different methods on how to solve partial differential equations. The implicit method is based on an equation systems that gives the configuration at the time t_{n+1} as a function of the later, current and previous steps.[14]

$$0 = f(x_{n+1}, x_n, x_{n-t}, ..., t_{n+1}, t_n, ...) \tag{2.48}$$

Since the system of equations is solved at every time step, the method needs both matrix inversion and iterative solution algorithms. An example of an implicit method is the backward Euler method seen in equation 2.49.[14]

$$y'(t) \approx \frac{y(t) - y(t-h)}{h} \tag{2.49}$$

Where y is a function of of time and t and h are time increments.

2.8.2 Explicit Method

The Euler method, or forward Euler method, is an explicit method and is a one-order numerical procedure that solve ordinary differential equations. From the previous state a small tangential increment is calculated with equation 2.50 to find the current state. The Euler forward is an explicit method meaning that it is solved with extremely small time steps using an linear approximation.[14]

$$y'(t) \approx \frac{y(t+h) - y(t)}{h} \tag{2.50}$$

The explicit method is often used for nonlinear dynamic problems where the effects of acceleration cannot be neglected. The method is often used in extreme scenarios such as a crash or a drop test. The scheme is not unconditionally stable and the method requires a smaller time step that is less than the Courant time step (i.e., the time taken by a sound wave to travel across an element).[14]

The differences between these methods will directly influence the accuracy and the computational time of the FEM simulation and it is therefore important to choose the method carefully based on the physics of the problem.[14]

An implicit method is time consuming when solving dynamic and nonlinear problems but it is a more stable solver and a larger step size can be chosen than for an explicit method. The implicit method is often used for time independent analyses and problems involving stiff behaviours, for which the use of explicit method would require small time steps to keep the result stable. For these problems, the use of implicit method result in less computational time because of the larger time step.[14]

3 Simulation Procedure

This chapter describes the simulation procedures from the forming simulation to the final plates assembled with the gasket. Procedure for two different approaches will be presented, the first by using ANSYS 2020 R2 and the second by using LS-PrePost V4.8.11. The chapter will explain steps in the procedure and will include limitations that is a part of the methods.

3.1 Current Method

The current method for the forming simulation at Alfa Laval is carried out in HyperMesh and DynaForm with LS-Dyna as the solver. The tools for the plate forming is first designed in Creo Parametic and then the simulation is performed in LS-Dyna in an explicit solver. The model is built in Dynaform. The material model used for the plates is Barlat 91 with a hardening curve defined with data from tensile tests performed at Alfa Laval. After forming the plate, a surface of the result is created in HyperMesh and is then imported to ANSYS to simulate the gasket behavior together with two plates. There is no connection between the two simulations more than the transferred surfaces of the formed plates which means that neither residual stresses, residual strains or material thinning is taken into consideration in the gasket simulation. The material models in ANSYS are not the same as in LS-Dyna and the material used for the plates in the gasket simulation is a predefined material with an isotropic multilinear hardening curve. The gasket is also imported in ANSYS with a predefined hyperelastic material model. The gasket simulation is solved implicitly in ANSYS Static Structural.

3.2 ANSYS workflow

As mentioned before, the task for this project is to develop a methodology on how to capture physical phenomenon. It is therefore important to choose an accurate material model but also to preserve the changes in the material from the first part of the manufacturing process, which is forming of the plates, to the final product. It was decided that the modelling of the forming and gasket simulation will be performed according to the current method with some changes that are necessary, meaning that for example mesh, velocity and contact definition will be defined according to the current method if possible but other materials will be used to fit the purpose of the project. For a seamless method and to ease the mapping of stresses and strains from the forming simulation to the gasket simulation, the entire methodology should be performed in the same software. The first attempt was to perform the simulations in ANSYS but to use the extended version ANSYS LS-Dyna for the explicit simulations.

3.2.1 Forming Simulation in ANSYS

The aim of this simulation was to get a result as close to the real forming process as possible. The current forming simulation in LS-Dyna is close to the real result. For the

current simulation, the whole workflow is not done in the same software and therefore, one of the simulations had to be implemented in a new software. ANSYS has a relatively new extension called ANSYS LS-Dyna where the first simulations of this project were performed. The model was implemented as similar to the LS-Dyna model as possible. A lot of the settings which are available in LS-Dyna were also available in ANSYS LS-Dyna. If the settings were not available a command could be added with a keyword from LS-Dyna. From Creo Parametic, a step-file was exported for the geometry. The geometry was opened in ANSYS LS-Dyna and a fine mesh was generated for the whole assembly, as seen in figure 3.1 and 3.2.

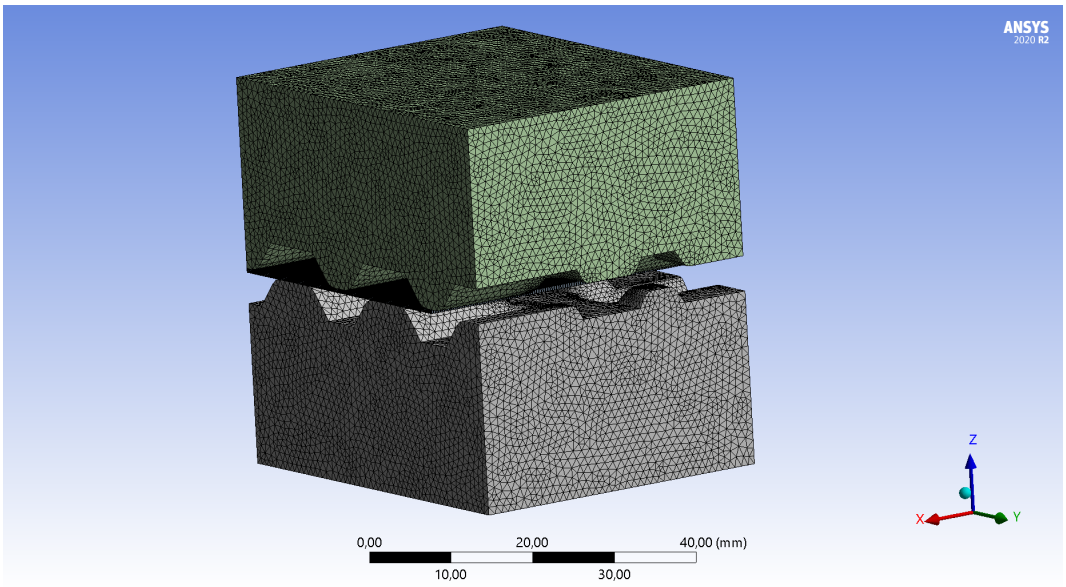

Figure 3.1: *Mesh for the model.*

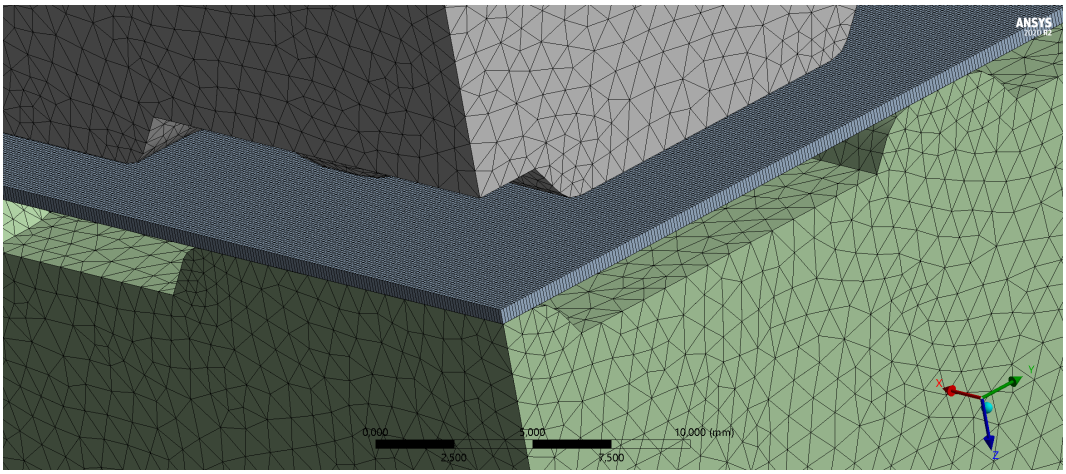

Figure 3.2: *Closeup on the mesh for the plate.*

Both the die and the stamp were set as rigid bodies whereas the die was fixed in all directions and the stamp was fixed in all directions except the z-direction where a velocity was applied,

figure 3.3. The velocity was applied as a sinus curve to get a smoothly varying load. The plate had a material model (Barlat 91 or Barlat YLD2000) imported as a command. The models were defined according to the keywords in LS-Dyna. A frictional boundary condition was set between the plate and the stamp and die.

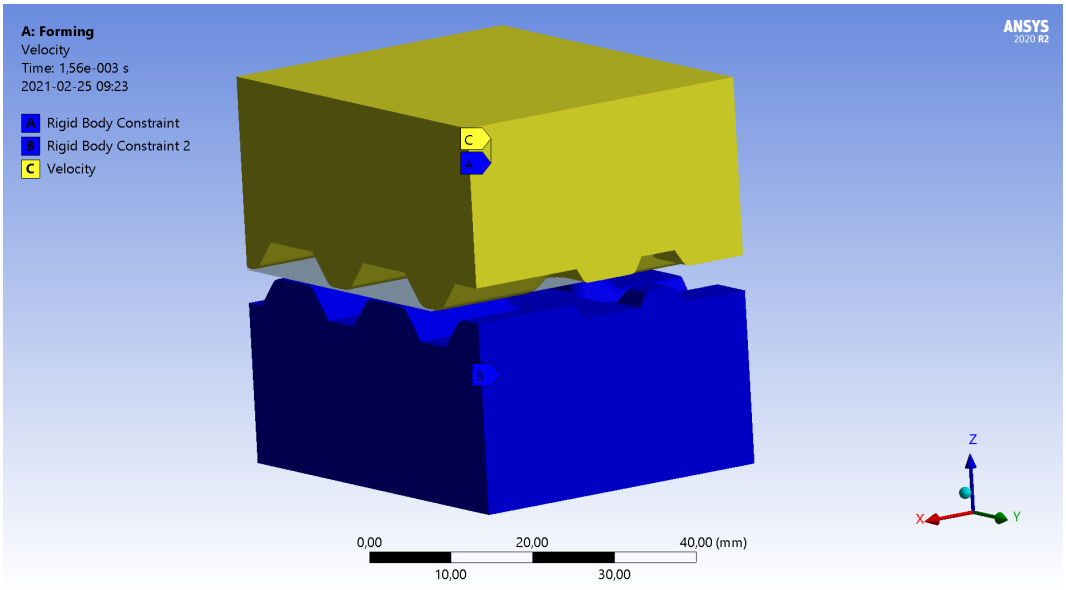

Figure 3.3: *Boundary conditions for the model.*

The forming simulation uses an explicit solver. Because of license issues, the ANSYS model had to be exported into a text file and solved in LS-Dyna analysis. The output file from the LS-Dyna analysis could then be imported into ANSYS again to show the results.

3.2.2 Gasket Simulation in ANSYS

The gasket simulations have already been developed in ANSYS as an implicit analysis and here the important part was to get the relevant data imported from the forming simulation. This data comprise the thickness, stress and strain for the plates. When trying to import these data files, a lot of problems arose. The first attempt was to drag the solution from the forming simulation to the setup for the gasket simulation. The thickness of the simulation was automatically imported. For the stresses and strains, they were imported as external data in csv-files. The mapping of the stresses and strains did not work as it should when loading them in the setup and they were not the same after mapping as they were before and the ANSYS support team said there was a bug in the software. The second attempt for importing the needed data was to import the whole model as a dynain-file. When importing the stresses and strains, an error occurred complaining that five integration points are needed. Even if five integration for the sheet were defined the software could only read three of those and this time as well, the ANSYS support team said that this was a bug in the software.

3.3 LS-Dyna workflow

When changing the solver to LS-Dyna, an easy step was to add a springback analysis in between the forming and gasket simulations which hopefully will give a valuable result without adding too much work. The difference between these simulations and the present simulations performed at Alfa Laval is that LS-PrePost is used as the pre- and postprocessing software for this procedure. The scheme in figure 3.4 shows the setup of the model in LS-PrePost.

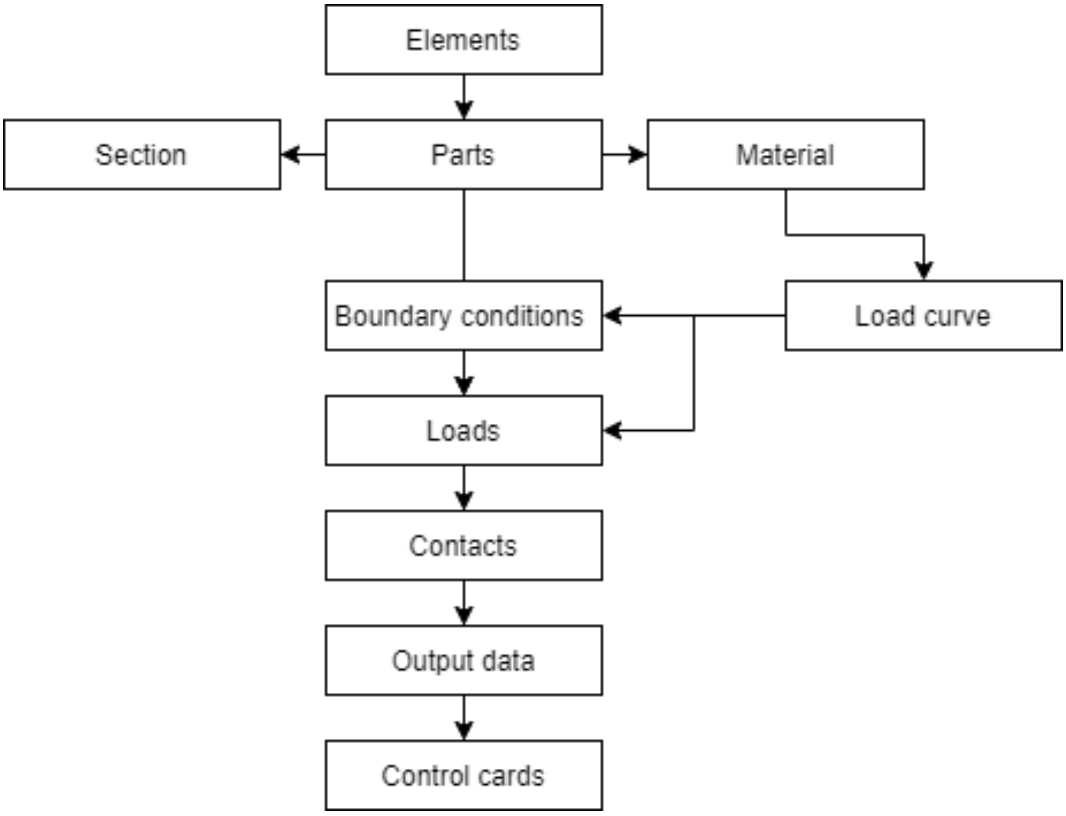

Figure 3.4: *Flow chart of the LS-Dyna workflow.*

3.3.1 Forming Simulation in LS-Dyna

The current simulation method at Alfa Laval already uses this forming simulation setup. The simulations follow the manual Alfa Laval has developed for a forming simulation. The forming simulation uses an explicit solver which is the default setting in LS-Dyna. First, the die and stamp were imported together with a blank. Materials were defined with the earlier mentioned material models. Both the die and stamp were set to rigid bodies. A velocity was added to the stamp as a sinus curve to get a smooth load. The setup for the plate, die and stamp is shown in figure 3.5.

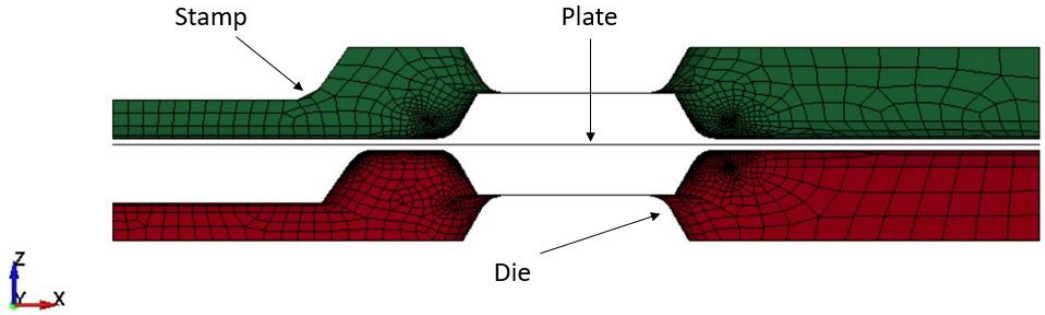

Figure 3.5: *Part setup for the forming simulation in LS PrePost. (Thickness of plates are not present in the figure.)*

Springback is a relatively easy simulation done in LS-Dyna and a small springback analysis was performed on the formed plates. The formed plate was imported as a dynain-file which means that both stress and strain are imported as initial loads. The springback analysis was an implicit analysis where one corner node was locked in all three directions, a second node was locked in y- and z-directions and a third node was locked in only the z-direction, figure 3.6. The number of integration points trough the thickness was varied to capture the springback behaviour and how it depends on the number of integration points.

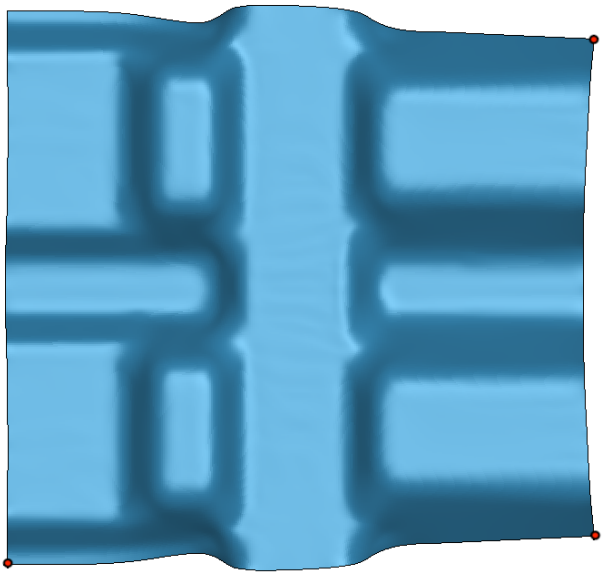

Figure 3.6: *Setup of plate where the nodes marked in red are the locked nodes.*

3.3.2 Gasket Simulation in LS-Dyna

The gasket simulation was performed as an implicit dynamics analysis. The plates were imported from a dynain-file which includes thickness, initial strain and initial stress. To avoid hourglassing in the plates, the shell elements in the plates were refined as fully integrated elements. The gasket were meshed in ANSYS since LS-Dyna has some problems with meshing solids. The shell elements are fully integrated and the shell has five integration points through the thickness and the solid elements in the gasket are under-integrated. Together with the gasket, two walls were imported as well to work as the outer force that will compress the gasket together with the two plates. A hyperelastic material model was defined for the gasket and the walls were set as rigid. The plates have the same material models as defined earlier.

A motion was added to the walls to compress the gasket until sealing. Between the gasket and the plates, frictional contacts were defined, and between the walls and the plates another frictional contact was defined. The setup for the gasket simulation in LS-Dyna are shown in figure 3.7.

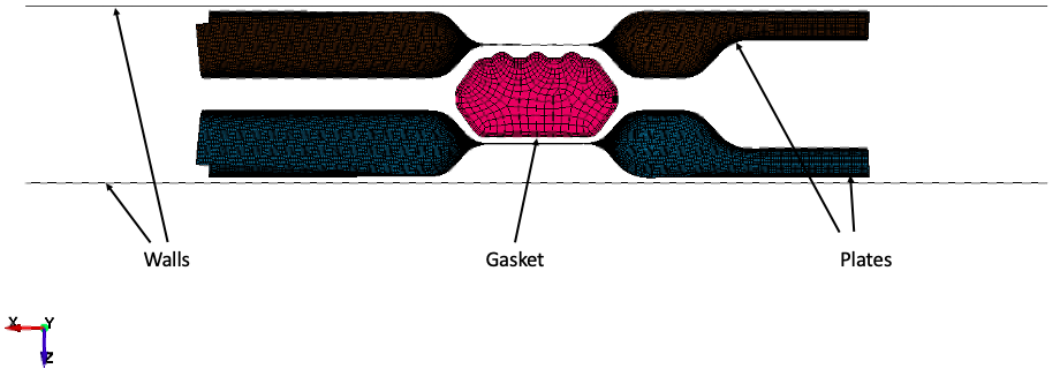

Figure 3.7: *Part setup for the gasket simulation in LS PrePost. (Thickness of plates are not present in the figure.)*

In the gasket some hourglassing occurred and to prevent this, hourglass control was set on the part as well as a refined mesh.

4 Results

The results in this chapter are based on the simulation procedures in chapter 3. The color bars in the figures are not present due to protection of Alfa Laval's data. The color scale is the same in each figure that shows stress and the results are comparable. The same goes for strain, the color scale is the same for all strain figures.

The values in the graphs and tables are also normalized due to protection of the data. All the graphs presenting stress are divided by the same value which means that they can still be compared. Likewise, the numbers in the tables are divided by the same value, which makes the numbers in the tables comparable.

4.1 ANSYS workflow

The forming simulations were successful in ANSYS and the results were similar to the LS-Dyna results in chapter 4.2. However, the following step which were mapping of the stresses and strains, did not work as it should. The results of the stress before and after mapping are shown in figure 4.1 and for strain before and after mapping in figure 4.2.

The stress after mapping are significantly lower than before mapping. Mapping of strain did not work at all and no strain was shown after the mapping was done. The pattern of the stress and strain before and after mapping should look the same and therefore the development of the workflow in ANSYS did not continue.

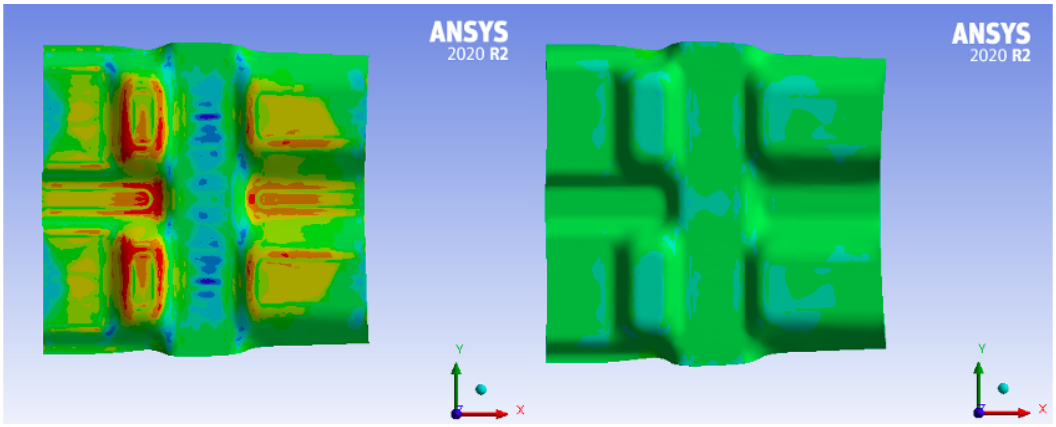

Figure 4.1: *Stress in y-direction before (left) and after (right) mapping. Red indicates high stress and blue low stress.*

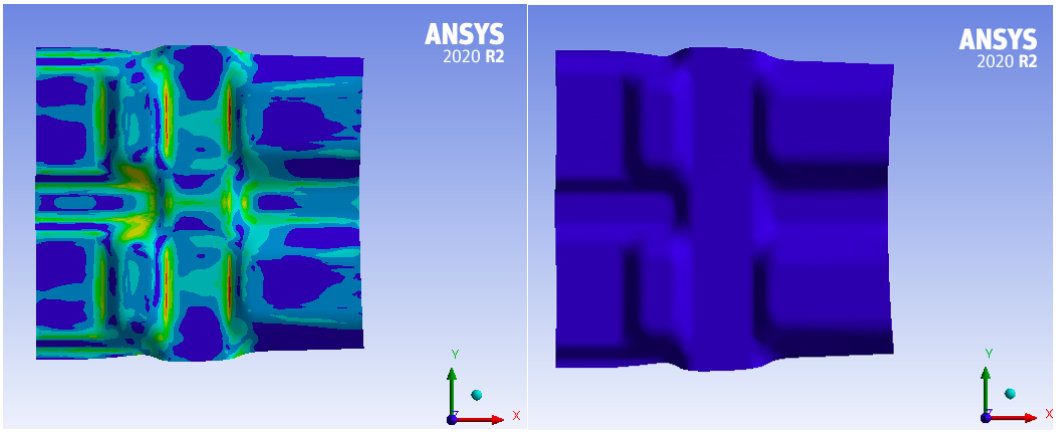

Figure 4.2: *Strain in y-direction before (left) and after (right) mapping. Red indicates high strain levels and blue low strain levels.*

4.2 Forming simulation LS-Dyna

For the forming simulations, the material models Barlat 91 and YLD2000 in combination with 5, 7 and 11 number of integration points (NIP) was used to analyse any differences in results depending on these parameters. The runtime for Barlat 91 where approximately 1.1 times faster than for YLD2000. The figures 4.3, 4.4, 4.5 and 4.6 shows the stress and strain distribution for the final formed plate with the material model Barlat 91 and five integration points. The stress and strain distribution for the remaining forming simulations will not be presented since the distribution pattern is similar to the plate presented below regardless of material model and number of integration points. The figures is instead supplemented with diagrams which demonstrates differences in stress and strain level throughout the forming simulation for the different material models and number of integration points.

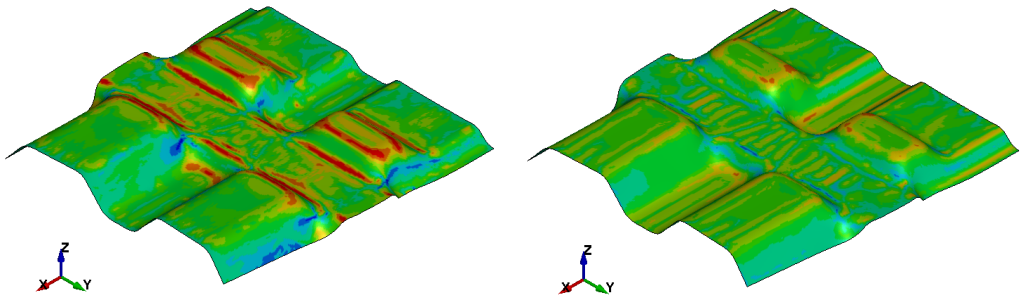

Figure 4.3: *Normal stress in x-direction (left) and y-direction (right) for five integration points for Barlat 91. Red indicates high stress and blue low stress.*

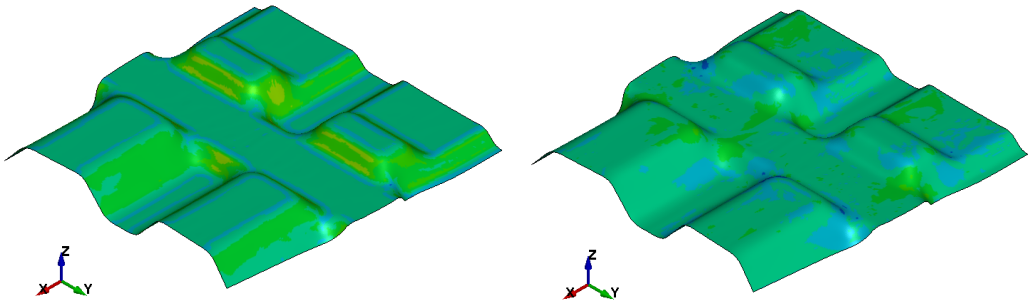

Figure 4.4: *Normal stress in z-direction (left) and shear stress in xy-direction (right) for five integration points for Barlat 91. Red indicates high stress and blue low stress.*

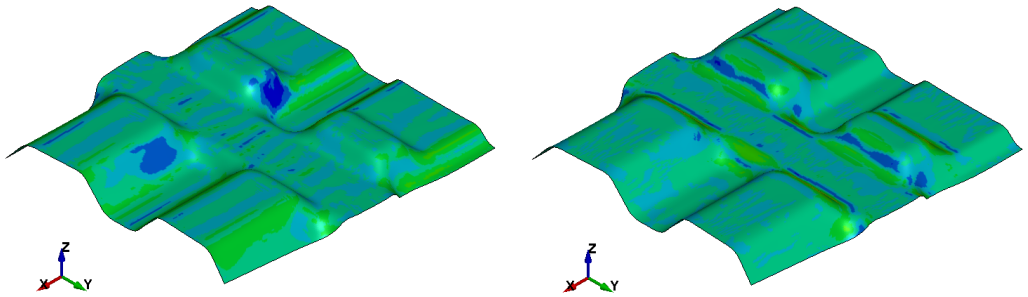

Figure 4.5: *Shear stress in yz-direction (left) and shear stress in xz-direction (right) for five integration points for Barlat 91. Red indicates high stress and blue low stress.*

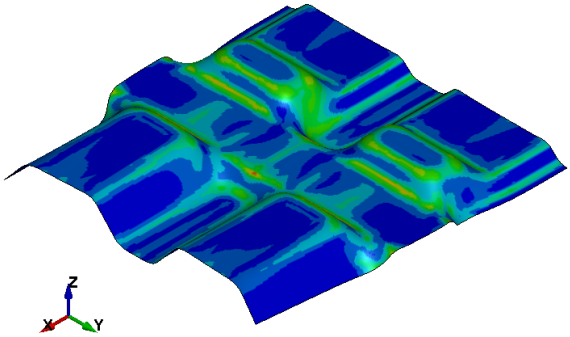

Figure 4.6: *Effective plastic strain for Barlat 91 for five integration points. Red indicates high strain levels and blue low strain levels.*

In the figures 4.7, 4.8, 4.9, 4.10, 4.11 and 4.12 the maximum value of stress in the forming simulations are shown at each time step. Lastly, the figure 4.13 present the effective plastic strain in each time step for the plate. The blue graphs are the Barlat 91 model and this is the model Alfa Laval uses today. Because of a simplified geometry in this dissertation, this result cannot be compared to a real formed plate.

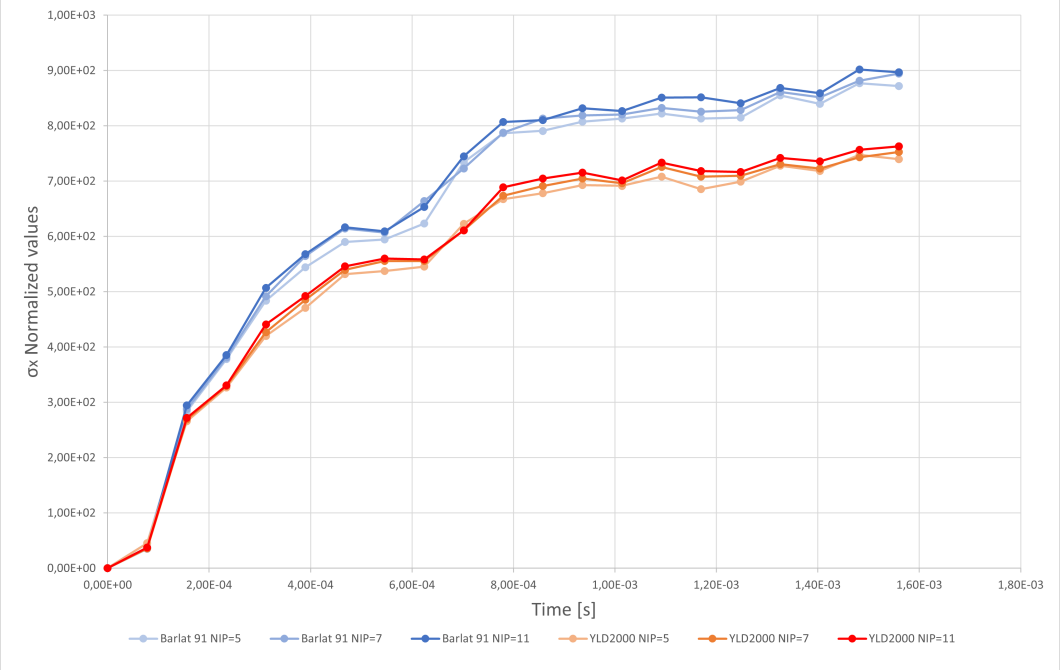

Figure 4.7: *The diagram presents the maximum normalized stress in x-direction for the plates with the material models Barlat 91 and YLD2000 and with 5, 7 and 11 integration points.*

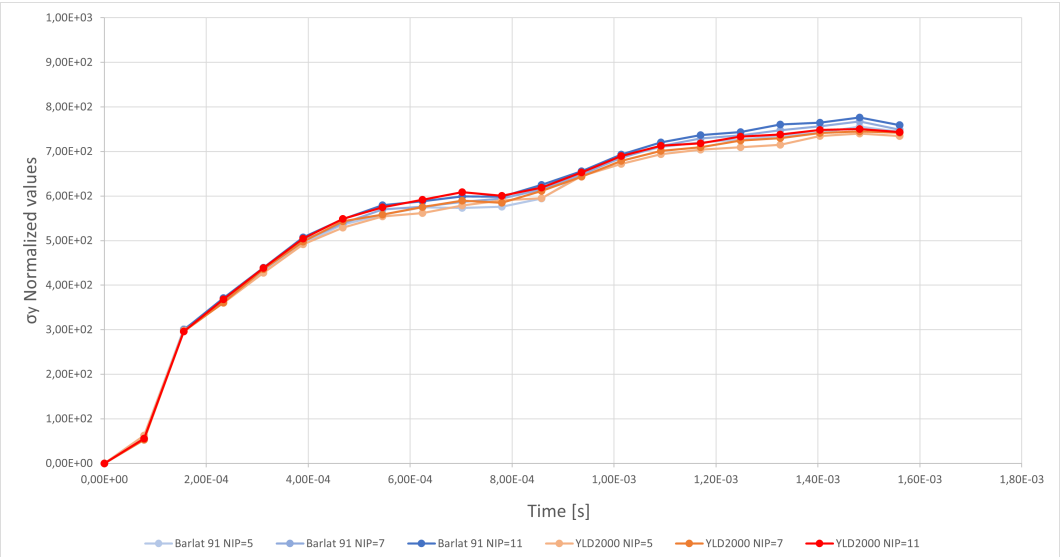

Figure 4.8: *The diagram presents the maximum normalized stress in y-direction for the plates with the material models Barlat 91 and YLD2000 and with 5, 7 and 11 integration points.*

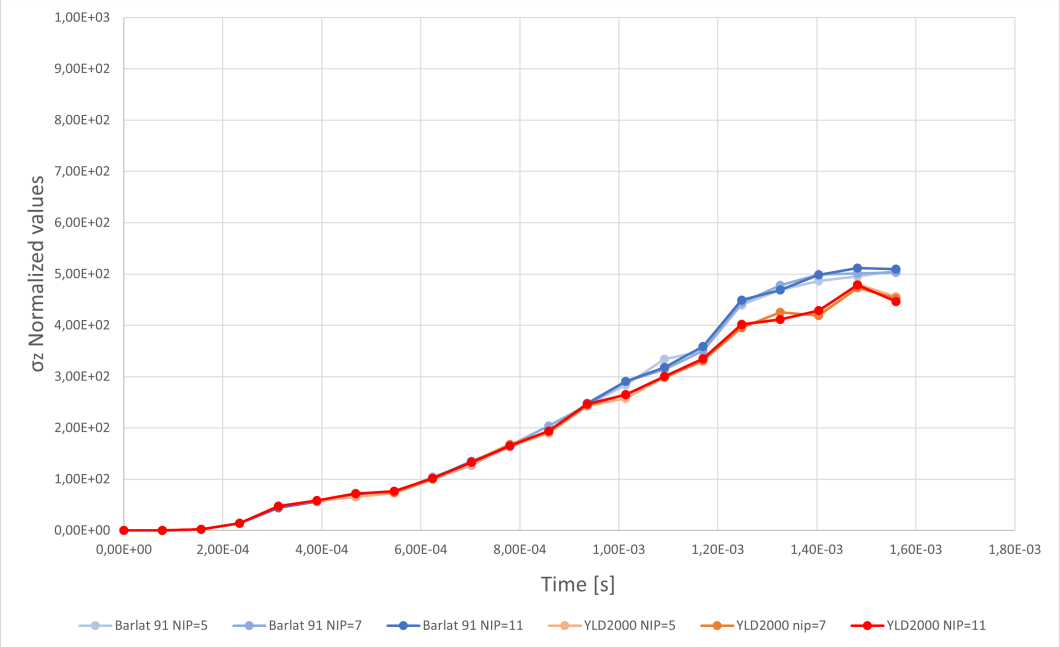

Figure 4.9: *The diagram presents the maximum normalized stress in z-direction for the plates with the material models Barlat 91 and YLD2000 and with 5, 7 and 11 integration points.*

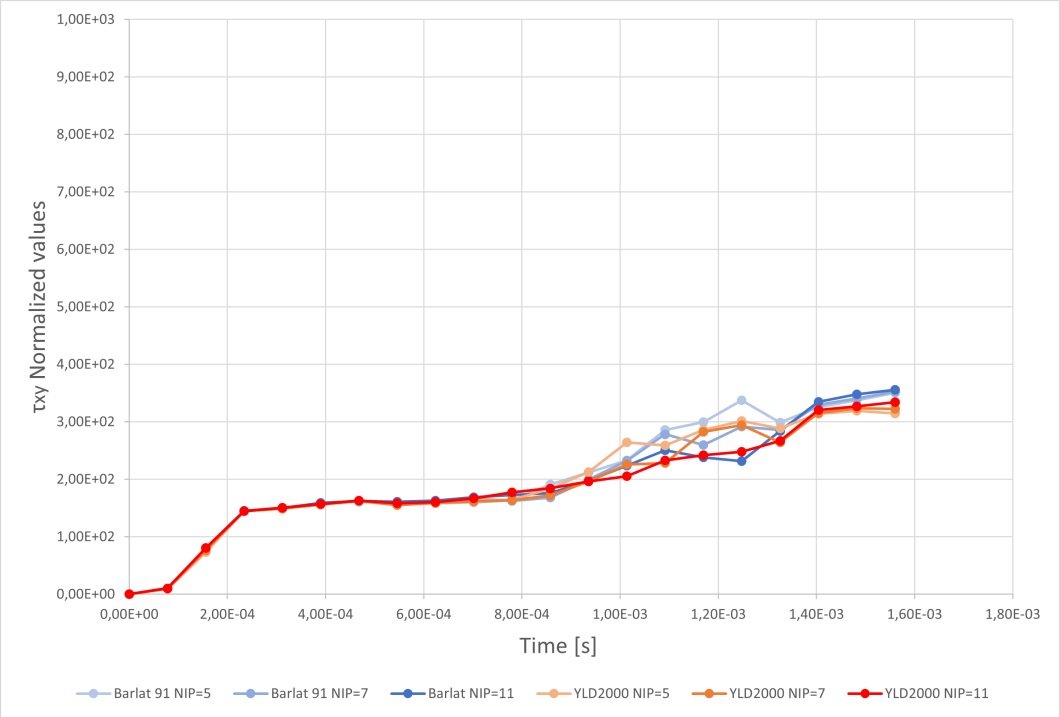

Figure 4.10: *The diagram presents the maximum normalized shear stress in xy-direction for the plates with the material models Barlat 91 and YLD2000 and with 5, 7 and 11 integration points.*

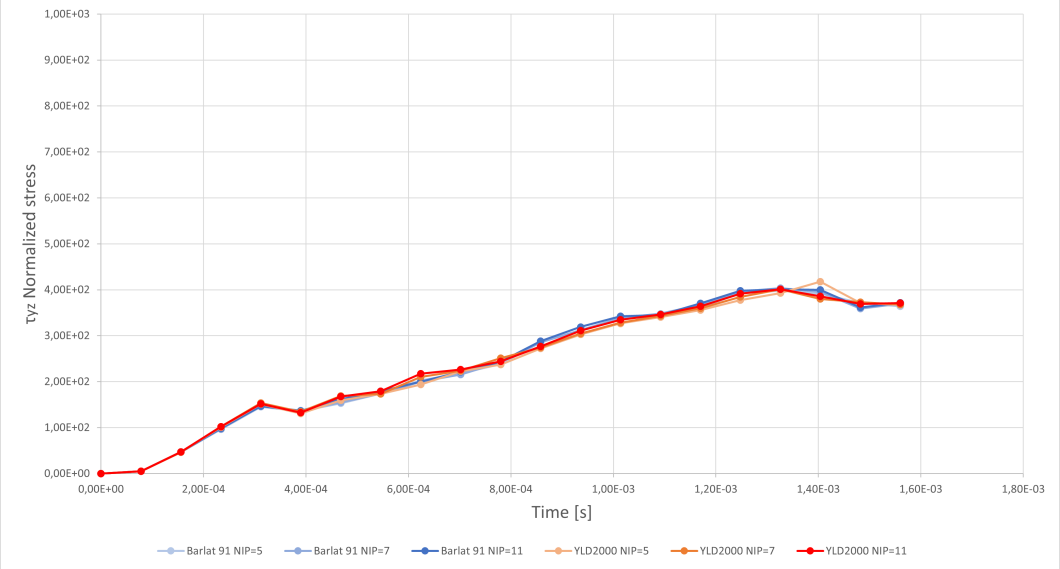

Figure 4.11: *The diagram presents the maximum normalized shear stress in yz-direction for the plates with the material models Barlat 91 and YLD2000 and with 5, 7 and 11 integration points.*

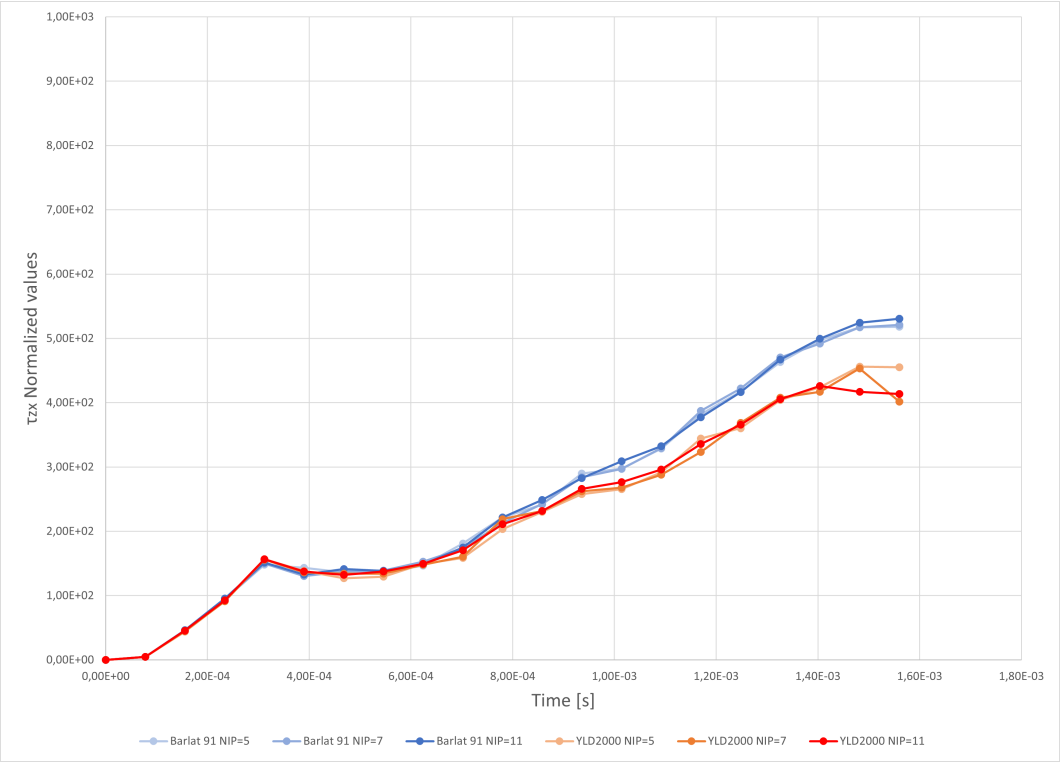

Figure 4.12: *The diagram presents the maximum normalized shear stress in zx-direction for the plates with the material models Barlat 91 and YLD2000 and with 5, 7 and 11 integration points.*

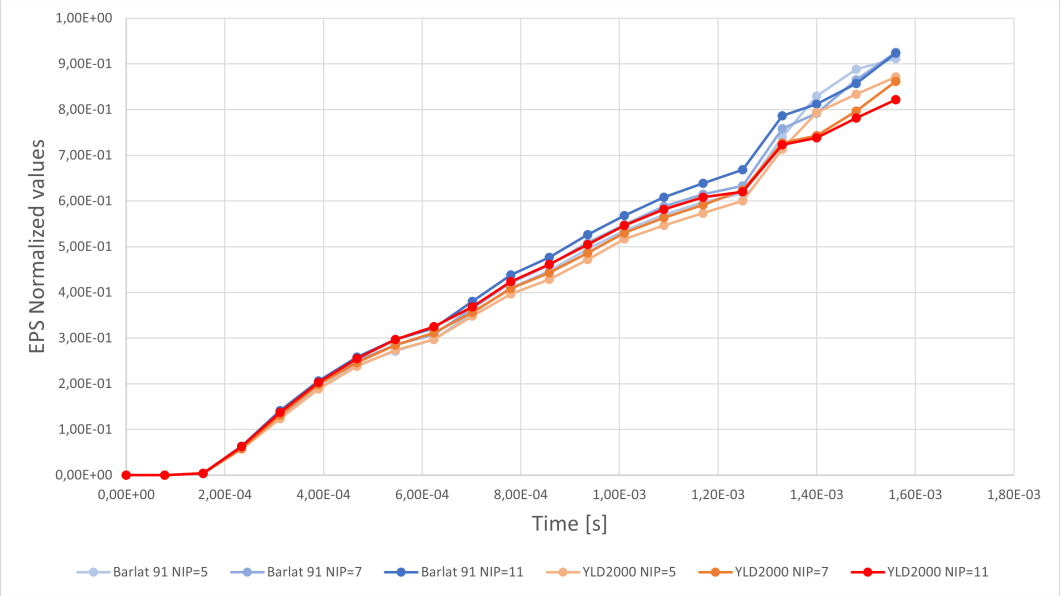

Figure 4.13: *The diagram presents the normalized effective plastic strain for the plates with the material models Barlat 91 and YLD2000 and with 5, 7 and 11 integration points.*

Figure 4.14 shows the thickness reduction for Barlat 91 with five integration points. There were only a negligible difference in thickness between the two material models and no difference between the integration points. Figure 4.14 represents thickness reduction for both material models and all integration points.

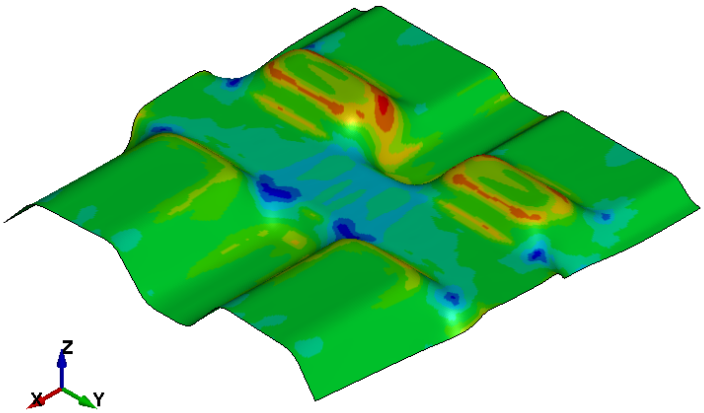

Figure 4.14: *Thickness of plate after forming simulation. Red indicates a decrease in material thickness and blue an increase in material thickness.*

4.3 Springback simulation LS-Dyna

For the springback simulations, different number of integration points (NIP) were tested. In figure 4.15 the displacement in x-, y- and z-directions for the two material models are presented. The node studied is marked in red in figure 4.16. Barlat 91 has a lower value in the x-direction and a higher value for y-displacement for all of the number of integration

points. The estimation in the z-direction for Barlat 91 differs a bit compared to YLD 2000. In the x-direction, the values do not vary as much and are more stable than for the y- and z-directions. For the springback simulations, YLD2000 was the most time efficient simulation and it was roughly 1.2 times faster than Barlat 91.

Figure 4.15: *Values of displacement in x-, y-, and z-directions for corner node in figure 4.16.*

	NIP 5		NIP 7		NIP 11	
Displacement	Barlat91	YLD 2000	Barlat91	YLD 2000	Barlat91	YLD 2000
x	2,986	3,169	2,925	3,117	2,884	3,167
y	0,376	0,280	0,426	0,297	0,306	0,138
z	0,203	0,259	0,329	0,118	0,249	0,263

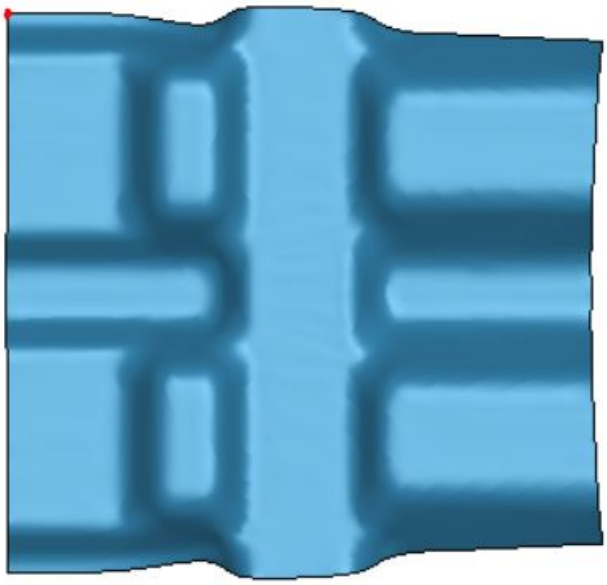

Figure 4.16: *The node marked in red is the node studied when analyzing springback.*

When doing a springback analysis the plate is unloaded from the die. This leads to a decrease in stresses. In figure 4.17 the percentage difference in stresses, before and after the unloading from the die, are presented. The residual stress after the unloading is shown in figure 4.18.

Figure 4.17: *Percentage difference for maximum value of stress before and after the springback analysis.*

	Barlat 91			YLD 2000		
	NIP = 5	NIP = 7	NIP = 11	NIP = 5	NIP = 7	NIP = 11
σx	-21,1%	-22,8%	-22,6%	-18,9%	-18,5%	-20,3%
σy	-32,5%	-30,4%	-28,2%	-34,6%	-35,2%	-35,3%
σz	-50,7%	-49,5%	-45,9%	-53,2%	-54,4%	-46,4%
τxy	-4,4%	-5,0%	-2,4%	-0,5%	-1,8%	-2,2%
τyz	-21,0%	-11,4%	-10,0%	-24,4%	-9,4%	-2,0%
τxz	-47,9%	-47,5%	-49,9%	-44,3%	-44,2%	-43,6%

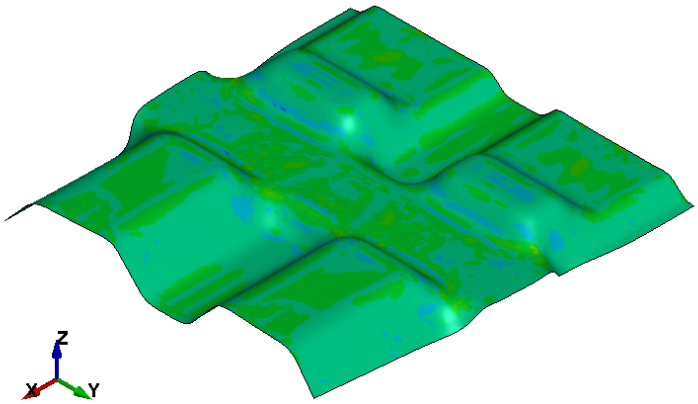

Figure 4.18: *Residual stress after springback analysis for a plate with five integration points and the material model 91.*

4.4 Gasket Simulation

Both material models for the plates were considered in the gasket simulation. Here the runtime for Barlat 91 was 1.2 times faster than for YLD2000. The displacement applied on the walls lead to a compression of the gasket. In figure 4.19 the maximum principal stress are shown for both models.

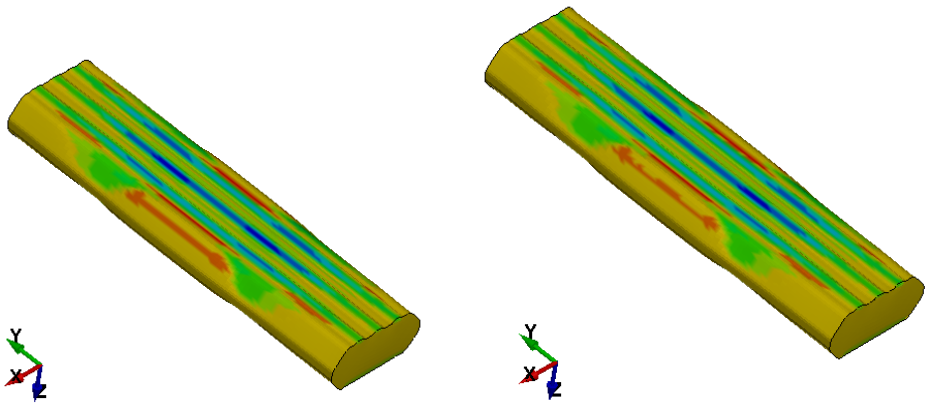

Figure 4.19: *Maximum principal stress for the gasket with Barlat 91 plate (left) and YLD 2000 (right).*

In figure 4.20 the initial stress for the plate before compression of the gasket is shown. Like the previous figures, the plate presented is with five integration points and the material model Barlat 91. The initial stress is a result from mapping of the residual stress in the springback analysis.

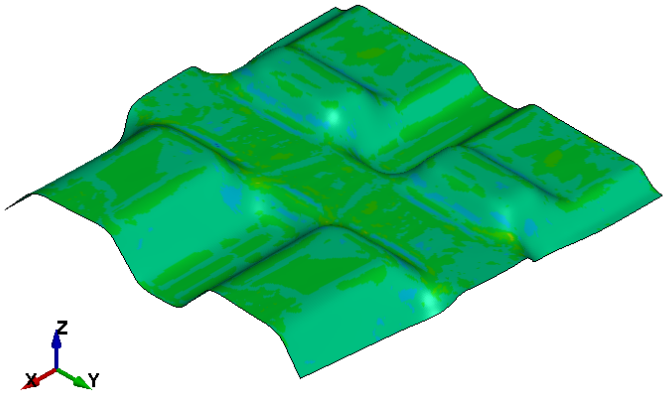

Figure 4.20: *Initial stress before gasket simulation for a plate with five integration points and the material model Barlat 91.*

Figure 4.21 shows effective plastic strain for material model Barlat 91 before compression with gasket. This figure can be compared with figure 4.6 which is the effective plastic strain after forming.

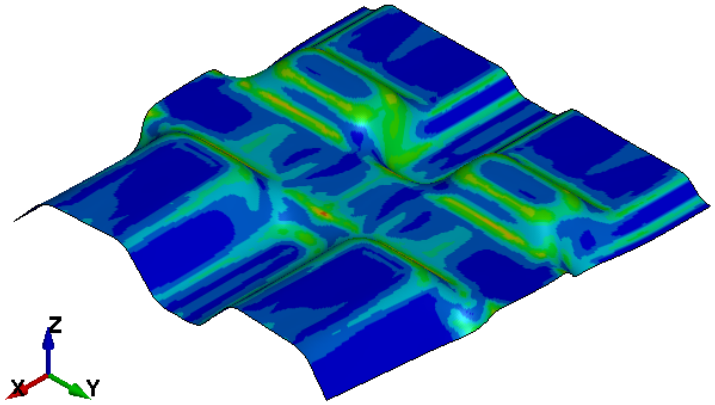

Figure 4.21: *Effective plastic strain for Barlat 91 in gasket simulation for one plate before compression.*

After compression of the gasket, plastic strains are still present in the plates and are shown in figure 4.22. The plastic strain is mainly a result from the forming of the plate.

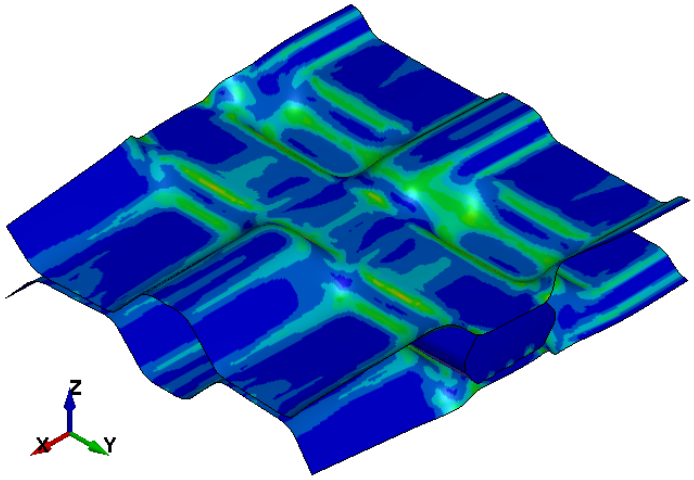

Figure 4.22: *Effective plastic strain for the plates with Barlat 91 material model after gasket compression.*

5 Discussion

The following chapter includes discussion of the simulation procedure in chapter 3 and the results in chapter 4. Findings and problems that occurred during the project are also presented. The last sections include a conclusion and our thoughts on future work for the analysed methodology.

5.1 ANSYS Workflow

As previously mentioned, the attempt of an ANSYS workflow was unsuccessful mainly due to bugs in the software but also due to license problems. This section will discuss possible pros and cons with the ANSYS workflow and can of course only draw conclusions based on our work and not for a working ANSYS workflow, where more problems might occur.

Starting with the cons of this workflow. An important part of this task was to accurately capture material phenomenon which meant that it was essential to choose a material model that was well suited for the analysis and described the actual behavior of the material. Early in the process, we discovered that LS-Dyna had more alternatives when choosing a material model and ANSYS was limited especially with anisotropic material. The new extension ANSYS LS-Dyna allowed commands from LS-Dyna to be imported, which allowed the forming simulation to be performed in the desired material model. However, for the gasket simulation performed in ANSYS static structural we had to use another material model with a multilinear hardening curve which we believe would not be as accurate as the Barlat models. The con for this workflow is to either choose two different material models or to use the same ANSYS material from forming to gasket simulation, which may not be as accurate.

We mentioned in the method section that there were two methods on how to import the geometry and the result from the forming simulation to the gasket simulation, both which had bugs and problems. The first alternative, to first drag the solution cell to the model cell and then exporting the stresses and strain had problems with mapping the imported stress and strain. Nonetheless, the method was also rather complicated compared to the other alternative since all six stress components had to be exported from the result as a text file and then imported as external data where it was important that the data was read accurately from the text file. From this aspect, creating a dynain-file with the results included and then importing it to the gasket simulation would be a more seamless solution if it would have worked.

A final disadvantage was the postprocess in the extended version ANSYS LS-Dyna, where we were only able to study effective plastic strain. No other properties such as the elastic strain components in the x-, y- and z-direction, which was probably a limitation from the extension not being fully developed in ANSYS yet.

Although we had difficulties with finalizing the workflow in ANSYS, we could still see some advantages with using ANSYS instead if LS-Dyna. The main advantage was the user interface, which was preferable in ANSYS as it was more user-friendly compared to the

alternative. When the software is updated, we see users that are only familiar with ANSYS choosing this workflow which previously was divided into two software. Another advantage is the meshing of solids which was considerably easier in ANSYS.

5.2 LS-Dyna Workflow

The LS-PrePost simulations were more successful than the ANSYS simulations. As previous stated, the forming simulations were already developed in Dynaform, which is similar to LS-PrePost and the same keywords could be used. The forming simulation was successful and the strains and stresses were saved for further use. The import of initial strain and stress for subsequent simulations was easily done and did not need any extra work.

Even though the interface is easier in ANSYS, there are more possibilities in LS-Dyna and the LS-Dyna software is adapted for sheet metal forming.

The keyword-files used in LS-Dyna is also a big benefit, it is easy to make small changes by just correcting in the keyword-file instead of opening the whole model in LS-PrePost, especially when changing between different integration points.

5.2.1 Forming Simulation

The forming simulation considered both Barlat 91 and YLD2000. The result differ between the two material models. Barlat 91 has slightly higher stress levels than YLD2000. When defining the material models, the hardening curve imported is defined in y-direction which reasonably gives the result in figure 4.8 where all curves overlap. In x- and z-direction, as well as the shear stress, the estimations differ between the models.

Looking at the curves in figures 4.7-4.12 we can see that there are only a slight difference between the curves that represents the same material models but different number of integration points. The number of integration points trough the thickness does not have a big impact on the result in the forming process but will probably give a more valuable result for the springback analysis.

The thickness reduction in figure 4.14 shows that the material is thinner around the spherical corners. There were no difference between the material models for thickness reduction. YLD2000 is a more expensive model for forming analysis, however the estimation of the thickness with Barlat 91 is just as good as YLD2000. When only looking at material thickness there is no point of using a more complex material model.

5.2.2 Springback Simulation

In the result from the springback simulations there is a difference between the two material models and also between the different number of integration points. Firstly, we look at the integration points and draw the conclusion that even though there is a difference in the results, there is no linear relation between the number of integration points and the value of displacement in the different directions. Secondly, looking at differences between the NIP

for Barlat 91 the x-displacement is more stable than y- and z-displacement. The same goes for YLD2000.

The residual stress from the springback analysis is significantly lower than the stress levels after the forming simulation, as seen in figure 4.17. The figure presents the percentage differences in stress levels from before and after springback of the plate. From the numbers, it follows that the biggest change is for stresses in the z-direction and shear stress in xz-direction. This seem reasonable because the plate has deformed most in the z-direction and because of the geometry of the plate.

Springback is a phenomena that is hard to predict and the springback phenomena will probably affect subsequent results and will be a valuable step towards a physically realistic simulation. We did not have the time to compare the results from the springback analyses with the real formed plate and therefore we cannot conclude which of the material models or number of integration points that are best suited with only simulations. In theory, more integration points are known to give a better approximation and YLD2000 is developed to be better at estimating springback than its precursor Barlat 91.

5.2.3 Gasket Simulation

The most important result for this dissertation, is that the material change from the forming simulation should be present in the plates in the gasket simulation. The history of the material is considered when the developed stress and strain from every step of the process contributes to the final result which is confirmed by studying the mapping of the stresses and strains. The formation of plastic strains is mainly developed during forming simulation and will not increase nor decrease during springback analysis. This means that in a correct mapping of this quantity, the strains from the forming simulation should be equal to the strains at gasket simulation before the plates is compressed with the gasket. When comparing the figure 4.21 from the gasket simulation with figure 4.6, we can see that the strain is exactly the same. However, the stresses in the gasket simulation can not be compared with the result from the forming simulation since the stress level changes in the springback analysis. During springback of the plate, the stress level is lowered leaving only the residual stresses on the plate. To confirm the correct transfer of stresses, the initial stress for the gasket simulation is compered with the final stress in the springback simulation. Figure 4.20 shows the initial stress in y-direction on the plate and figure 4.17 shows the residual stress from springback. When comparing these figures, we see that the quantities is correctly transferred throughout the simulations.

With the correct mapping, we can see in figure 4.22 the plastic strain developed during forming, springback and compression is present at the final simulation for the plate. In comparison to the current method used at Alfa Laval where the plates showed no plastic strains from forming or springback at the final simulation. If plastic strain is present in the result it is from the compression of the gasket, which is a significantly small contribution to the total plastic strain.

In figure 4.19 there are small differences for the principal stress between Barlat 91 and YLD2000. The simulations are performed with the same setup and the only differences are

the material models and the results from the springback simulations. As seen in section 4.3 there are some differences in the springback result between the two models and this leads to the plates having slightly different geometrical appearance. When using these plates in the gasket simulations the compression for the gasket wont be exactly the same. There are only small differences, however analysing the gasket deformation was out of scope for this project.

A disadvantage with LS-Dyna is the solid meshing that comes with some problems. The meshing of solids is better in ANSYS and therefore we used this instead. This comes with some extra work that could be avoided if using ANSYS instead.

5.3 Conclusion

The purpose of this dissertation was to develop a finite element analysis methodology that will process the history of the material from coil to fully formed plate mounted in a heat exchanger. To start off, the ANSYS workflow did not work as we have hoped and there were a lot of difficulties that made us change software to LS-Dyna. Moreover, the forming simulations went much better in LS-Dyna and the results seemed reasonable compared to forming simulations previously done at Alfa Laval.

The springback simulations are relatively easy to perform and we believe that estimating springback will contribute to a more beneficial result in the end. The displacements and the change in stress shows that springback of the plate changes the geometry when releasing the plate from the die which of course will affect further simulations. To conclude how the springback simulations will affect the final result, physical tests have to be performed to verify the springback analysis.

The final simulation is the plates compressing the gasket where the result is important for a working methodology. The previous section, section 5.2.3, discussed a successful mapping of the stresses and strains which means that it is a working procedure in LS-Dyna. The procedure is rather straight forward and is considered to be a seamless methodology. The analysis suggested improvements for higher accuracy by presenting a new material model and increased number of integration points. None of the results can imply which and if the changes is better than the current analysis but the changes should improve the results in theory and the analysis states that there are differences in result.

To conclude, the ANSYS workflow could in the future be a better option for these simulations. The interface is easier in ANSYS, but the extension for LS-Dyna is not developed enough to actually use it as we wanted to. Therefore, the LS-Dyna workflow is recommended for this type of analysis and for any further development of this methodology. More data from practical tests are necessary to draw conclusions on the best setup and material model for the analysis.

5.4 Future Work

To further develop this method, the material directions relative to the rolling direction should be considered as rolling of sheet metal provides a highly anisotropic material behavior. With the correct angles, both for the diagonal to the rolling direction and for the beams going out from the diagonal, the simulated formed plates can be compared with a scanned formed physical plate to see how good the estimations are. Especially in the different directions to catch the anisotropy in the material. Anisotropy due to the rolling will also affect thinning during and after forming as well as springback behaviour.

Another interesting thing to consider are the two material models and look closer if there are any benefits with the newer YLD2000 when estimating springback. However, springback is a material behaviour that is hard to predict and there might not be any significant differences between the two material models.

The new methodology is more expensive but will hopefully get an approximation closer to the real result. However, no work has been performed on decreasing the runtime for the simulations. Suggestions on areas to investigate is if it will be necessary to use fully integrated shell elements in the gasket simulations or to re-mesh the plates for the different simulations.

6 References

1. Alfa Laval, 'Vad är Alfa Laval?', accessed 2021 February 2, https://www.alfalaval.se/om-oss/our-company/

2. Alfa Laval, 'Packningsförsedda värmeväxlare', accessed 2021 february 15, https://www.alfalaval.se/microsites/packningsforsedda-plattvarmevaxlare/

3. Alfa Laval, 'Plate design', accessed 2021 february 15, https://www.alfalaval.com/microsites/gphe/tools/plate-types/

4. Ottosen, N., Petersson, H., 1992, 'Introduction to the finite element method', *Prentice Hall*, Great Britian.

5. Ristinmaa, M., 'Introduction to Non-linear Finite Element Method', 2019, Division of Solid Mechanics, Lund University

6. Ottosen, S.N., Ristinmaa, M., 2005 'The Mechanics of Constitutive Modelling' *Elservier Ltd* 1st ed. Great Britain

7. Guo, X., Xu, H., Zeng, Q., Pet, T., 2021, 'Springback characteristics of arched aluminum alloy gusset plate after stamping forming', *Thin-Walled Structure* Vol 159

8. Jacques, N., 2020, 'An analytical model for necking strains in stretched plates under dynamic biaxial loading', *International Journal of Solids and Structures* Vol 200-201, pp. 198-212

9. LS-Dyna, 2020, 'LS-Dyna Keyword user's manual - Volume I', *Livermore Software Technology*, pp. 11.1-11.119 18.93-18.101, 18.113-18.120

10. Barlat, F., Lege, D.J., Brem, J.C., 1991, 'A six-component yield function for anisotropic materials', *International Journal of Plasticity* Vol 7, pp 693-712

11. Barlat, F., Brem J.C., Yoon J.W., Chung K., Dick R.E., Lege D.J., Pourboghrat F., Choi S.H., Chu E., 2003, 'Plane stress yield function for aluminium alloys sheets: part 1 - theory', *International Journal of Plasticity* Vol 19, pp 1297–1319

12. Hunter, D.B., 1972, 'Some Gauss-type formulae for the evaluation of Cauchy principal values of integrals', *Numerische Mathematik*, Vol 19, pp. 419-24

13. Jabareen, M., Rubin, M. B.,2007, 'Hyperelasticity and physical shear buckling of a block predicted by the Cosserat point element compared with inelasticity and hourglassing predicted by other element formulations', *Computational Mechanics*, Vol 40, pp. 447-459

14. Yang, D. Y., Jung, D.W., Song, I.S., Yoo, D.J., Lee, J.H., 1995, 'Comparative investigation into implicit, explicit, and iterative implicit/explicit schemes for the simulation of sheet-metal forming processes' *Journal of Materials Processing Technology* Vol 50, pp. 39-53